2 Ocular Imaging for Enhancing the Understanding, Assessment, and Management of Age-Related Macular Degeneration

Marco Nassisi and Srinivas R. Sadda

Abstract

Age-related macular degeneration (AMD) is a progressive neuro-retinal disease and the leading cause of central vision loss among elderly individuals in the developed countries. Modern ocular imaging technologies constitute an essential component of the evaluation of these patients and have contributed extensively to our understanding of the disease. A challenge with any review of ocular imaging technologies is the rapid pace of progress and evolution of these instruments. Nonetheless, for proper and optimal use of these technologies, it is essential for the user to understand the technical principles underlying the imaging modality and their role in assessing the disease in various settings. Indeed, AMD, like many other retinal diseases, benefits from a multimodal imaging approach to optimally characterize the disease. In this chapter, we will review the various imaging technologies currently used in the assessment and management of AMD.

Keywords

Age-related macular degeneration · Geographic atrophy · Macular neovascularization · Optical coherence tomography · Optical coherence tomography angiography · Dye-based angiography · Fundus photography · Fundus autofluorescence · Adaptive optics · Widefield imaging · Multimodal Imaging

List of Abbreviations

AMD	Age-related macular degeneration
AOSLO	Adaptive optics scanning laser ophthalmoscopy
CC	Choriocapillaris
CFP	Color fundus photography
cORA	Complete outer retinal atrophy
cRORA	Complete retinal pigment epithelium and outer retina atrophy
EDI	Enhanced depth imaging
EFC	Emission fluorescence components
EZ	Ellipsoid zone
FA	Fluorescein angiography
FAF	Fundus autofluorescence
FLIO	Fluorescence lifetime imaging ophthalmoscopy
GA	Geographic atrophy
ICGA	Indocyanine green angiography
iORA	Incomplete outer retinal atrophy

M. Nassisi · S. R. Sadda (✉)
Doheny Image Reading Center, Doheny Eye Institute, Los Angeles, CA, USA

Department of Ophthalmology, David Geffen School of Medicine at UCLA, Los Angeles, CA, USA
e-mail: SSadda@doheny.org

E. Y. Chew, A. Swaroop (eds.), *Age-related Macular Degeneration*, Advances in Experimental Medicine and Biology 1256, https://doi.org/10.1007/978-3-030-66014-7_2

IRF	Intraretinal fluid
iRORA	Incomplete retinal pigment epithelium and outer retina atrophy
LED	Light-emitting diode
MFP	Multicolor fundus photography
MNV	Macular neovascularization
NIR	Near-infrared reflectance
OCT	Optical coherence tomography
OCTA	Optical coherence tomography angiography
ORT	Outer retinal tubulation
PCV	Polypoidal choroidal vasculopathy (aneurysmal type 1 neovascularization)
PED	Pigment epithelium detachment
PRPD	Peripheral reticular pigmentary degeneration
qAF	Quantitative autofluorescence
RPE	Retinal pigment epithelium
SD-OCT (A)	Spectral domain optical coherence tomography (angiography)
SLO	Scanning laser ophthalmoscopy
SRF	Subretinal fluid
SS-OCT (A)	Swept source optical coherence tomography (angiography)
TD-OCT	Time domain optical coherence tomography
SW-FAF	Short wavelength fundus autofluorescence

2.1 Background

Advances in imaging have dramatically affected our assessment of age-related macular degeneration (AMD). The high definition and high magnification of certain imaging modalities such as optical coherence tomography (OCT) or adaptive optics scanning laser ophthalmoscopy (AOSLO) have allowed the in vivo visualization of the retinal tissue, comparable to histologic samples. Thus, the opportunity to study the disease in all its phases and phenotypes has yielded new insights into the pathophysiology of AMD.

Multimodal approaches using different modalities in an integrated fashion have been a key strategy for clinical assessment. In fact, the combination of cross-sectional and en face images obtained simultaneously through OCT devices equipped with a confocal scanning laser ophthalmoscope (SLO) allows a microscopic correlation between clinical, anatomical, and pathological findings in multiple conditions [1–3].

Once diagnosed, AMD is a lifelong condition that requires accurate assessment and potentially long-term management [4]. Current treatment approaches (in clinical practice or clinical trials) largely target advanced stages of the disease like macular neovascularization (MNV) and geographic atrophy (GA). In the near future, treating AMD earlier in the disease course could increase the likelihood of the preservation of vision, while significantly improving the cost-effectiveness of drug treatments and reducing the costs of drug development.

Different mechanisms have been proposed to be relevant to the development of AMD including oxidative stress, accumulation of lipofuscin in retinal pigment epithelium (RPE), and primary damage to Bruch's membrane [5–7]. These microstructural alterations progressively lead to the early clinical findings of the disease, including features such as RPE depigmentation, drusen, and RPE hyperplasia. Eventually, complete outer retinal, RPE and choriocapillaris (CC) atrophy may develop, resulting in the late stage of dry AMD: geographic atrophy (GA). On the other hand, the sudden and often unpredictable development of neovessels, under the stimuli of vascular endothelial growth factor (VEGF) and other inflammatory factors, leads to MNV marked by exudation, bleeding and, eventually to fibrosis and atrophy with poor visual outcomes if left untreated.

Traditionally, disease grading relies on the photographic evaluation of the fundus, with the determination of the extent of drusen as well as the presence of pigmentary abnormalities in the posterior pole [8–12]. The advent of digitalization, together with new imaging technologies, provides often a higher sensitivity and has facilitated an automated or semiautomated quantitative analysis of all the features that might be considered at risk for the development and the progression of AMD [13–15].

A proper imaging assessment is fundamental in clinical therapeutic trials for advanced AMD as it can influence patient selection, and overall duration, costs, and outcomes of the studies. Given the rapid advance of new devices and post-acquisition image analysis algorithms, the selection of appropriate imaging modalities can be challenging. Currently, a multimodal approach is broadly accepted as the gold standard for imaging assessment of AMD patients [1, 2].

2.2 Color and Multicolor Fundus Photography

Color fundus photography (CFP) captures an image of the retina, with various degrees of fidelity with respect to clinical fundus ophthalmoscopy, depending on the different machines and modalities. It allows the early detection of a broad range of pathological changes associated with the early (i.e., drusen, lipids, crystalline deposits, and alterations of pigmentations) or late stages (i.e., hemorrhages, fluid, exudates, atrophy and fibrosis) of AMD. Multicolor fundus photography (MFP) is relatively newer technology and provides a "false color" image of the fundus combining three different wavelengths of light. The relative ease and tolerability of acquisition of these modalities offer important advantages to the management of AMD patients. Furthermore, digital photographs offer the possibility of post-processing analysis, paving the way to the development of automated algorithms for quantification of AMD-related features. This will be an important step forward for the early detection of disease and its monitoring.

2.2.1 Color Fundus Photography

Historically, CFP has always been considered the gold standard to demonstrate fundus alterations. Fundus cameras are designed to provide an upright, magnified view of the fundus using a white flash for illumination. A typical camera views 30–50° of retinal area, with a magnification of 2.5×.

A series of crucial improvements to fundus photography have been made over the last decades, such as nonmydriatic imaging, electronic illumination control, automated eye alignment, and high-resolution digital image capture [16]. This has contributed to advanced fundus photography as an essential tool in clinical practice to document retinal pathologies, and its use is often considered mandatory in disease definition and classification.

CFP is also considered the gold or reference standard for the evaluation of newer imaging technologies, and it is currently in use in clinical studies of AMD. During the last decades, several groups have proposed AMD classification systems based on CFP [8, 17]; the most recent of which utilize the presence of fundus pigmentary abnormalities (either hypo or hyperpigmentation) and drusen size to distinguish early, intermediate, and late AMD.

The latest classification was proposed in 2013 by the Beckman Initiative for Macular Research Classification Committee: early AMD was defined as medium drusen (i.e., between 63 and 125 μm) and no associated pigmentary abnormalities. Intermediate AMD demonstrated large drusen (i.e., >125 μm) and/or any AMD pigmentary abnormalities. Finally, the presence of MNV and/or GA was the key findings associated with the late stages of the disease [18].

This staging does not take into account the type of drusen present, with regards to features other than size. The relatively low contrast of the color photographs sometimes makes the identification of AMD-associated abnormalities challenging. Soft and cuticular drusen are easily visualized in CFP as diffuse spots with variable shades of yellow, depending on their constitution and the health of the overlaying RPE that can variably attenuate the blue light [19]. On the other hand, subretinal drusenoid deposits (SSD, aka reticular pseudodrusen (RPD) [20]), which are important risk factors for AMD progression [20–22], can be challenging to detect as they overly the RPE and are not affected by the RPE-related filtering of blue light. In fact, without

additional processing, CFP has a relatively low sensitivity for SSD detection (range: 33–42%).

The presence of MNV in CFP is also challenging to recognize, and signs of exudation and bleeding generally must be present to facilitate detection (Fig. 2.1). Previous studies report a sensitivity for the detection of MNV using CFP of about 78%, which drops to 38% when CFP alone is to be used to determine whether the MNV is active or not [23]. A multimodal approach implementing dye (i.e., FA and ICGA) and/or nondye-based (i.e., OCT and OCT angiography [OCTA]) techniques is therefore essential.

On the other hand, GA lesions are more easily identifiable on CFP and in fact the classic definition of GA is based on a qualitative and a quantitative evaluation of CFP images. The International Age-Related Maculopathy Epidemiological Study Group defined GA as any sharply delineated roughly round or oval area of hypopigmentation or depigmentation with increased visibility of the underlying choroidal vessels and of at least 175 μm in diameter on 30° or 35° CFP images [17].

Nevertheless, CFP is also limited for the purpose of measuring GA precisely owing to difficulty in delineation of the boundaries of lesions, specifically in case of relatively smaller size and multifocality.

The stereoscopic acquisition with CFP can provide higher sensitivity to detect topographic alterations at the periphery of atrophic regions and/or the presence of fluid and pigment epithelial detachment (PED). On the other hand, stereoscopic imaging is not always feasible, even in clinical trials, as it requires good cooperation from patients, and it should be performed by operators with senior experience.

2.2.2 Multicolor Fundus Photography

Multicolor images are generated from the simultaneous use of three different wavelengths: blue reflectance (wavelength: 488 nm), green reflectance (wavelength: 518 nm), and typically NIR (wavelength: 820 nm) [24]. The resulting three reflectance images are then combined into a "multicolor" image, also defined as "pseudocolor" or "false-color" image since it is not the result of the whole visible light spectrum but only of the sum of three wavelengths. Multicolor imaging systems use SLO techniques for image acquisition. In SLO systems, a confocal aperture is designed to clear backscattering light from outside the focal plane, making possible the imaging of individual layers of the retina with higher contrast and spatial resolution than with previous approaches [25].

The three different light wavelengths used in MFP can gather distinctive information from the various layers of the retina, as they penetrate them to different extents. In particular, the short wave reflectance (blue) highlights the inner retina and the vitreoretinal interface; green reflectance enhances the examination of the deep structures of the retina; and, finally, NIR facilitates the visualization of the choroid and the outer retina [24].

At present, a small number of report regarding this innovative modality have been published [22, 26, 27], and the findings in AMD are highly correlated with CFP. In the context of GA, the borders of the lesion are better visualized because of the higher contrast of the MFP (Fig. 2.2) [27].

Furthermore, fibrotic alterations and hemorrhages can be easily detected because of their optical reflection properties; however, subtle hemorrhages can sometimes be misjudged for pigmentary lesions using only MFP alone.

While CFP is more susceptible to media opacities and poor mydriasis because of the use of high-intensity and broad-spectrum light, it is possible to acquire high-quality multicolor images through nondilated pupils. However, the blue spectrum can be adversely affected by media opacities and poor mydriasis as well, influencing in an unpredictable way the signal strength of the resulting image [28].

A recent interesting addition to the available instruments for CFP is a new confocal device using white light. This machine (CentervueEidon; Centervue, Padova, Italy) offers the advantages of providing a "true color" image of the fundus, with increased contrast because of its confocality (Fig. 2.3) (using slit rather than circular confocal pinhole) [29]. However, no large studies comparing these confocal white-light color images with standard CFP have yet been performed.

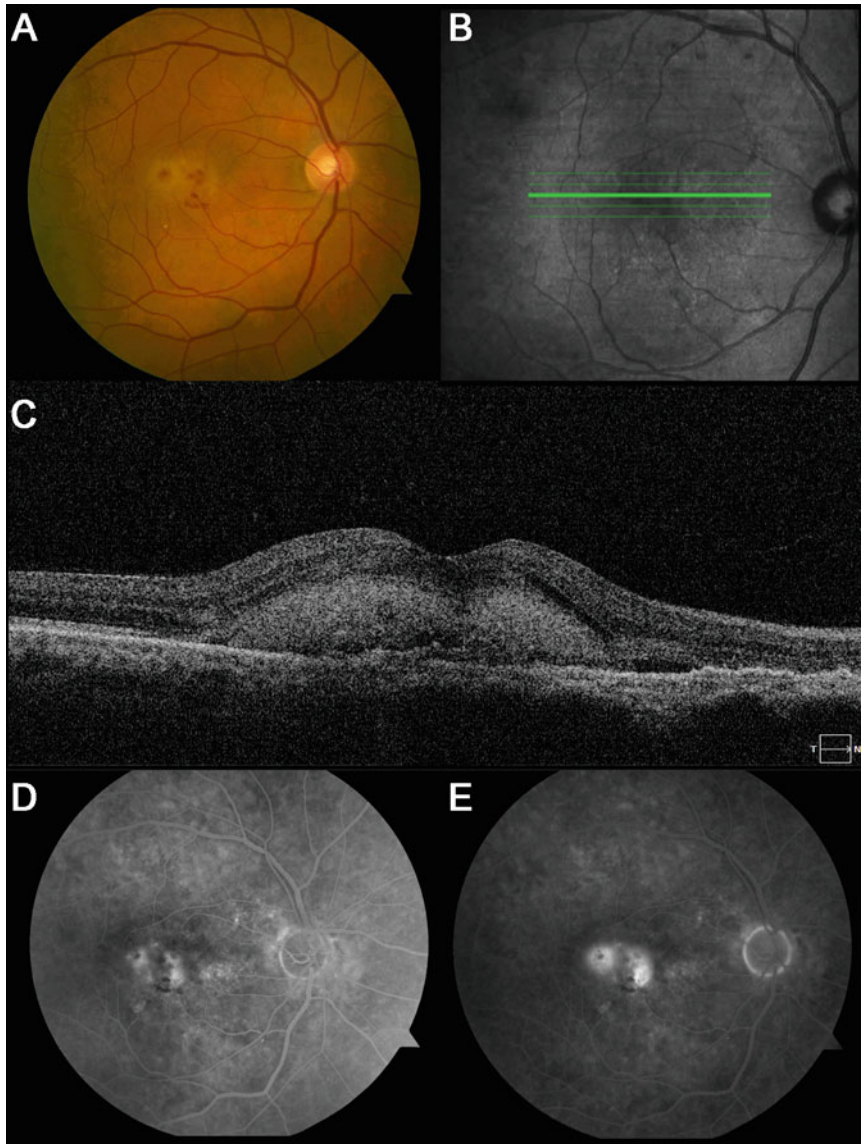

Fig. 2.1 Multimodal imaging of a patient with macular neovascularization (MNV) secondary to age-related macular degeneration in the right eye. In the color fundus photograph, (**a**) hemorrhages suggest the presence of MNV, which is confirmed by optical coherence tomography (OCT, infra-red reference (**b**) and B-Scan (**c**)). The B-Scan (**c**) shows a type 2 MNV (subretinal hyperreflective material) with subretinal fluid. The fluorescein angiogram shows a classic MNV (with some blockage from the hemorrhages) in the early phases (**d**) with evidence of dye leakage later in the exam (**e**)

2.2.3 Near-Infrared Reflectance

In AMD, most of the information needed for the evaluation of the fundus is gathered by the NIR (Fig. 2.2). Indeed, it has not been specifically investigated if using the two additional wavelengths could enhance or hide any details in the MFP image.

The NIR SLO image has little interference and absorption by media opacities and the luteal pigment in the macula providing high contrast, above all for lesions involving the fovea. Near-

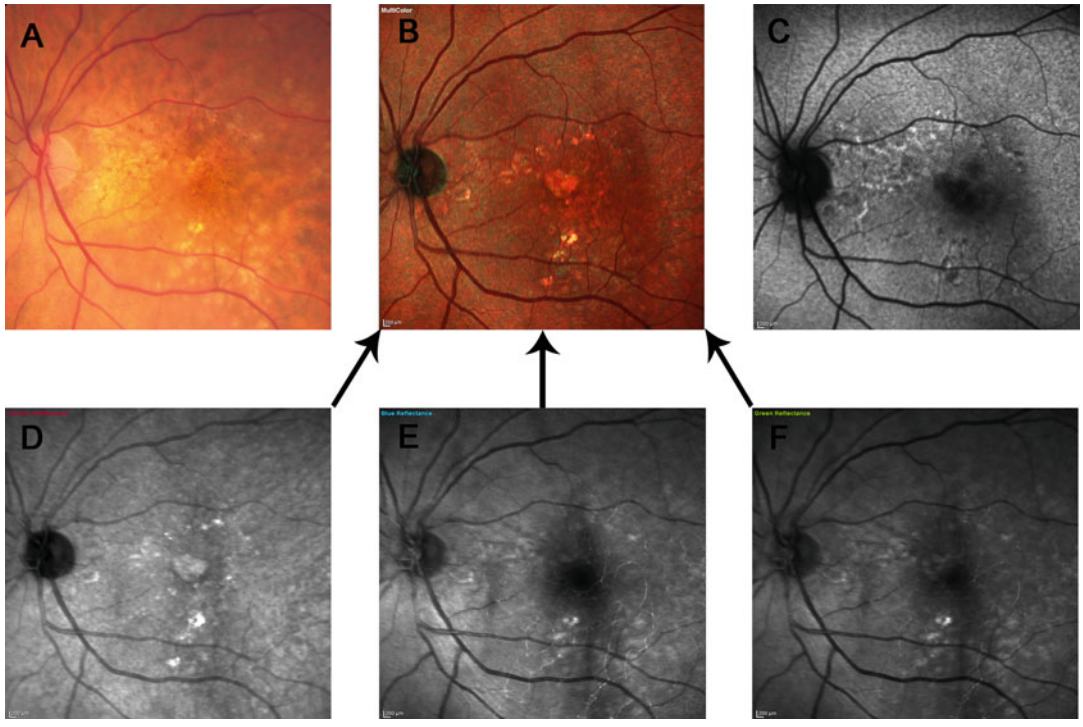

Fig. 2.2 Color fundus photograph (**a**), multicolor fundus photograph (**b**), and short-wavelength fundus autofluorescence image (**c**) of a patient with geographic atrophy and drusen secondary to age-related macular degeneration (AMD). The definition and contrast of the lesions are enhanced in the confocal image (**b**) that allows the precise identification of all atrophic foci similar to what is possible with the autofluorescence image. The confocal multicolor image is the result of the sum of three different wavelengths: near-infrared reflectance (**d**), blue reflectance (**e**), and green reflectance (**f**). Among the three, the near-infrared reflectance gathers most of the information about the (AMD) lesions as they are deep to the retina, and it seems the least affected by media opacities (floaters in this case)

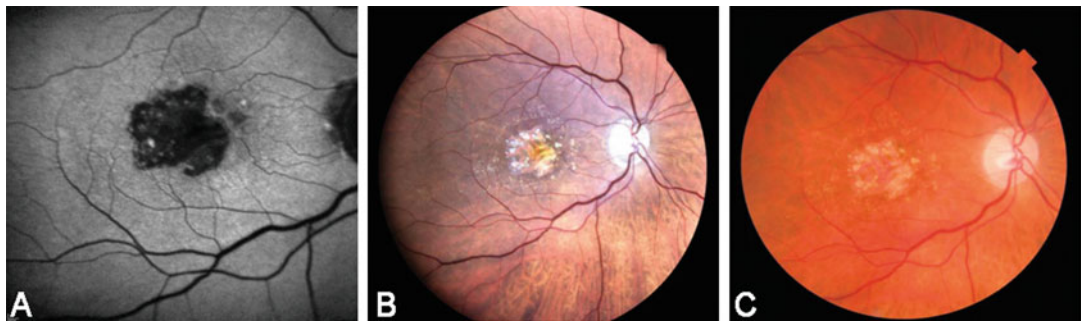

Fig. 2.3 Age-related macular degeneration patient with geographic atrophy, imaged by three different modalities: short wave-length fundus autofluorescence (**a**), confocal white-light fundus photography (**b**), and traditional color fundus photography (**c**). The confocality appears to enhance the contrast and details of the fundus image, allowing a better demarcation of the atrophic lesion

infrared light can better capture subretinal characteristics [30]; hence, NIR is the modality with the highest sensitivity for the detection of reticular pseudodrusen [20].

Three subtypes of SDD have been recently described by a recent study using multimodal imaging analysis: (1) dot pseudodrusen are usually located in the superior perifovea and appear

as small whitish deposits regularly arranged that correspond to small hyporeflective spots in NIR; (2) ribbon pseudodrusen (reticular pattern); (3) peripheral pseudodrusen are more uncommon and usually appear as yellowish aggregates that correspond to hyper-reflective spots in NIR images and are just outside the perifoveal region. Each subtype may have a specific composition, which may result in different hazards for the progression toward later stages of the disease [31].

NIR was first designed as a tool to guide the OCT acquisition; but later evolved to an independent output imaging technique (with a range of wavelength between 750 and 840 nm).

Accurate drusen assessment benefits from the use of infrared imaging as infrared light has deeper penetration in tissue and is less absorbed by media opacities, which are common in elderly patients [30]. Furthermore, the fraction of the infrared light that is scattered from the fundus may be detected using specific capture systems in "retromode" [32]. These systems are based on the different positions of the aperture which in "retromode" is not central (as in the standard systems), but it is lateral (right or left) and ring-shaped. "Retromode" imaging better highlights the deep retinal structures and the RPE [33], giving to elevated structures (e.g., drusen) a characteristic pseudo-3D "surface relief" pattern that makes their edges more visible.

2.3 Fundus Autofluorescence

Since its first description in the late 80s by Delori, fundus autofluorescence (FAF) has rapidly spread and become an invaluable tool for retinal evaluation [34]. This imaging modality allows the detection of fluorophores, which are natural molecules that interact with lights, absorbing and emitting it at specific wavelengths. The use of these specific wavelengths excites specific fluorophores that thereby become detectable. Specifically, melanin and lipofuscin can be detected using near-infrared (NIR-FAF) and short-wavelength (SW-FAF) light, respectively. Two systems are currently used to acquire FAF images: SLO systems and flash fundus camera-based systems. The former provides FAF images with enhanced contrast, resolution, and quality as they are able to suppress autofluorescence from anterior structures such as the crystalline lens. Given the unique information provided by FAF, its scope and clinical applications have expanded, and it is a particularly valuable tool for assessment of atrophic AMD.

2.3.1 Short-Wavelength Fundus Autofluorescence

Short-wavelength fundus autofluorescence has been the most well-studied FAF technique, and applications for many retinal diseases have been proposed. SW-FAF utilizes blue-light excitation (500–750 nm range), which is mostly adsorbed and emitted by lipofucsin, a dominant fluorophore located in the RPE. Pupil dilation and opacity of the media may affect the signal, influencing SW-FAF imaging quality. Furthermore, macular pigments intercept blue light, resulting in a drop in the intensity of the signal at the level of the fovea.

In SW-FAF, the intensity of the signal is mainly influenced by the quantity of lipofuscin. The alterations may be hypo-, iso-, or hyper-autofluorescent [35]. In the early stages of dry AMD, SW-FAF can demonstrate a larger affected area in comparison to color photography or fundoscopy. Pigment abnormalities on ophthalmoscopic exam may correspond to either hypo or hyper-autofluorescence based on their lipofuscin content [36]. Depigmented, hypoautofluorescent spots correlate with RPE atrophy, an early finding of GA [36, 37]. Recently, the International FAF Classification Group described eight different SW-FAF phenotypes that could be associated with early dry AMD: normal, minimal change, focal increase, patchy, linear, lace-like, reticular, and speckled [38]. These patterns may have clinical relevance as they may predict the development of late AMD stages and in particular choroidal neovascularization. Previous studies have suggested that the patchy, linear, and reticular patterns have the strongest correlation with progression to neovascular AMD [39, 40].

Similar to fundus photographs, drusens' features may widely vary in FAF imaging, according to size, composition, or condition of the overlying RPE and ellipsoid zone (EZ) [19, 41]. Large drusen may produce FAF alterations, whereas smaller drusen can appear iso-autofluorescent and may not be detected [42]. Intermediate drusen (diameter ranging between 63 and 125 μm) show a typical central hypo-autofluorescence surrounded by a ring of hyper-autofluorescence corresponding to the condition of the overlying RPE [43]. Cuticular and crystalline drusen appear hypo-autofluorescent with FAF [19] while soft confluent drusen tend to appear as hyper-autofluorescent lesions [42]. It should be highlighted that although these manifestations are the most common, drusen can show a plethora of FAF patterns.

Fundus autofluorescence may aid in the identification of two important features of high risk progression that could be problematic for detection by CFP or MFP: (1) drusenoid PED show a typical appearance of hyper-autofluorescent spots with a hypo-autofluorescent halo, but may be characterized by intermediate to decreased signal in case of overlying RPE atrophy or fibrovascular scarring [44]; (2) subretinal drusenoid deposits [20] were first reported as dot-like lesions by blue light photography and may be better visualized by SW-FAF, NIR-FAF, or OCT [44, 45]. These usually show the appearance of small and round, elongated foci of hypo-autofluorescence connected by interspersed reticular pattern of hyper-autofluorescence [46].

In general, early choroidal neovascularization may be not visualized on SW-FA, as RPE and photoreceptor layers are often relatively intact [47]. Subsequently, both types 1 and 2 MNVs may appear hypo-autofluorescent for different reasons: in type 2 MNV, the hypo-autofluorescence may be the effect of light blockage by the fibrovascular complex overlying the RPE in the subretinal space (Figs. 2.4 and 2.6); in type 1 MNV, the hypo-autofluorescence may be owed to the overlying RPE atrophy (Fig. 2.4) [48].

Macular neovascularization shows a hyper-autofluorescent halo in 38% of cases that may be due to a window defect secondary to the photoreceptor loss or to an RPE proliferation [39]. Hemorrhages and exudates may vary their appearances according to their age: at first they absorb light, appearing hypo-autofluorescent, but then when they become organized, they may appear hyper-autofluorescent.

Advanced lesions with RPE atrophy (GA), with the local loss of lipofuscin, produce areas with a low to extinguished SW-FAF signal. Given the high contrast between the areas with intact and atrophic RPE, the border of these lesions are typically sharply demarcated (Figs. 2.2 and 2.3) allowing semiautomated or even automated measurements of their area [49]. Nevertheless, there are some important limitations: (1) when the borders of the lesion are close and/or involve the fovea, they may be difficult to visualize due to the interference by macular pigment; (2) inside the atrophy, there may be some residual SW-FAF signal, preserved by retained RPE cells or debris and basal laminar deposits [50, 51]; (3) a halo of hyper-autofluorescence may surround the GA lesions, indicating the presence of ongoing RPE cell dysfunction or vertically superimposed RPE cells. This halo was associated with variable levels of atrophy expansion [52, 53] and has been reported with various appearances: none, focal, diffuse, banded, and patchy. The diffuse and banded phenotypes are associated with a faster rate of atrophy enlargement.

Another challenge is to distinguish GA and MNV when both coexist, and a multimodal approach is often required to discriminate atrophy, fibrosis, hemorrhages, or hard exudates [54]. Indeed, a combined analysis of SW-FAF and NIR images and FA may help achieving a precise identification and assessment of the atrophy [54, 55].

The strong interest in SW-FAF imaging in the clinical and research environments is clearly justified by its ability to precisely assess atrophy in AMD and potentially predict its progression [56]. In fact, current clinical trials on AMD use SW-FAF to measure GA not only for the demonstrated reliability of the measurements [57], but also for its correlation with the visual

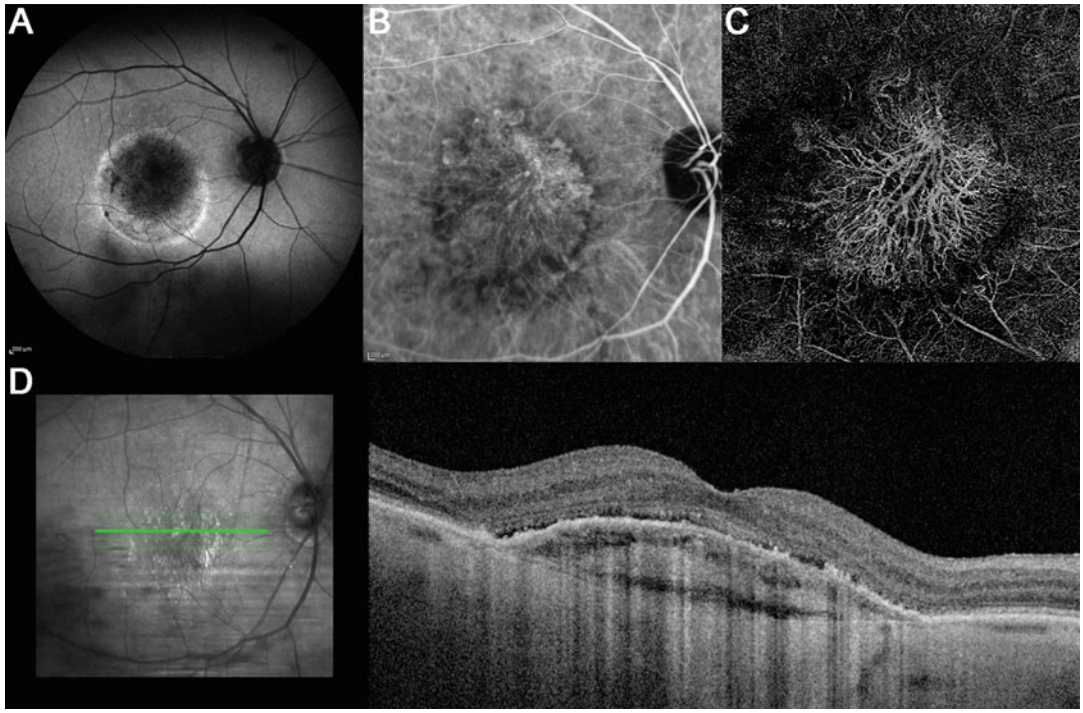

Fig. 2.4 Multimodal imaging of a patient with a type 1 macular neovascularization (MNV) secondary to age-related macular degeneration. The short wavelength autofluorescence (**a**) shows a round hypo-autofluorescent lesion (probably due to the subretinal fluid and overlying RPE atrophy) surrounded by a hyper-autofluorescent ring. Indocyanine green angiography (**b**) shows the neovascular network that perfectly corresponds to the enface optical coherence tomography (OCT) angiography image (**c**). OCT B-scan shows the location of the neovascular plexus between the retinal pigment epithelium and the Bruch's membrane

function; that is, when the autofluorescence signal is absent, it is correlated with a loss of retinal sensitivity [58, 59]. It should be noted, however, that in case of MNV, this assumption may not be completely accurate. Nevertheless, confluent patterns of autofluorescence loss in central macula are strongly related to visual acuity, contrast sensitivity, and reading speed in eyes treated with anti-VEGF agents for neovascular AMD [60, 61].

2.3.2 Near-Infrared Fundus Autofluorescence

Confocal SLO instruments can integrate multiple sources of light with different wavelengths, with a lower sensitivity to optical media opacities and macular pigment than SW-FAF. Confocal NIR-FAF (830 nm) is able to detect the melanin of the RPE and also, to some extent, melanin in the choroidal layers [62]. This has been confirmed by multiple animal and donor human eye studies [63]. In normal subjects, NIR-FAF is characterized a central area of high signal in correspondence of the foveal region, where the RPE are taller and thus have a higher concentration of melanin. This area of higher NIR-FAF corresponds to the physiologically reduced central SW-FAF [63, 64].

In early AMD, the correspondence between NIR-FAF and SW-FAF is not absolute, depending on the relative amount of lipofuscin and melanin in each lesion [65]. In eyes with neovascular AMD, the predominant finding is the blocking of NIR-FAF and SW-FAF by subretinal blood or MNV. The main difference is in areas of exudation activity where SW-FAF is

typically increased, whereas NIR-FAF is usually decreased [65].

For GA, the application of NIR-FAF can be complimentary to the SW-FAF due to some important differences: (1) the area of hypo-autofluorescence corresponding to GA atrophy is usually significantly larger in NIR-AF compared to SW-AF [65, 66]; (2) when the lesion is close to the fovea, SW-FAF might not have enough contrast for a distinct delineation of the borders, due to the masking effect of the macular pigment; (3) visualization of the borders of the lesion in NIR-FAF may also be difficult in pigmented individuals where the higher melanin signal from the choroid can reduce contrast [62]; (4) the fluorescence of the borders might be different between the two modalities: an iso-SW-FAF border may correspond to a hyper-NIR-FAF border—these areas are thought to have a persistent photoreceptor layer over an already damaged RPE, suggesting that NIR-FAF may detect areas of damaged RPE/photoreceptors cells earlier than SW-FAF [66].

Thus, optimally, a combination of both NIR-FAF and SW-FAF imaging should be implemented to detect and monitor morphological and functional RPE in AMD, especially in eyes with GA.

Several SLO and fundus camera systems implemented other wavelengths to investigate the retina; however, very few of them have been properly validated (i.e., 532 nm fundus cameras or 514 nm SLO systems) [67, 68]. A potential advantage of green FAF over blue FAF is that it is of lower energy and generally more comfortable for patients. The lower energy may also offer theoretical safety benefits, particularly in diseases eyes that may be more susceptible to light toxicity—however, this hypothesis requires careful study. A recent study compared green FAF versus blue FAF in measuring GA lesions, finding a slightly higher reproducibility and accuracy of measurements for green FAF. A post-hoc analysis related the inter-reader differences to the opacification of the media, which has a higher impact on the quality of the blue FAF compared to green FAF, hence affecting the precise grading of the lesions [69].

2.3.3 Color Autofluorescence

Recently, a confocal blue-light FAF device (CentervueEidon) using a 450 nm wavelength and a light-emitting diode (LED) light source has been introduced. The 450 nm wavelength is thought to excite different fluorophores from the ones excited with the classical 488 nm [70]. As this device is equipped with a color sensor, the full-spectrum of the emitted light can be detected, resulting in a "color FAF" image. This complete emission spectrum can be divided into long-wave and short-wave emission fluorescence components (EFC): "red" (560–700 nm) and "green' (510–560 nm). The evident advantage is that minor fluorophores, whose emission is usually overwhelmed by major ones (e.g., lipofuscin), could be isolated and studied as they emit in the shorter wavelength end of the spectrum (green EFC) [71, 72]. For example, in GA, while there is an absence (or major reduction) of the high red EFC component coming from lipofuscin, the green EFC signal is still present, even if diminished, and it seems to originate from subretinal hyper-reflective material. It is possible that drusen-like metabolites with highly glycated products have fluorescent capability and could be the source of this signal (Fig. 2.5) [72].

Thus, it is evident that 450 nm FAF imaging may yield further insights into the pathologic processes behind AMD pathogenesis and progression. However, more work is necessary to define the role of color FAF on the assessment and prognosis of AMD patients.

2.3.4 Quantitative Fundus Autofluorescence

While SW-FAF allows qualitative evaluation and quantitative measurements of areas of definite hypo- or hyper-autofluorescent alteration, traditional SW-FAF approaches do not allow the absolute FAF intensity to be quantified. A methodology that overcomes this limitation is quantitative autofluorescence (qAF), which employs an internal fluorescent reference to calculate the intensity of the autofluorescence of the

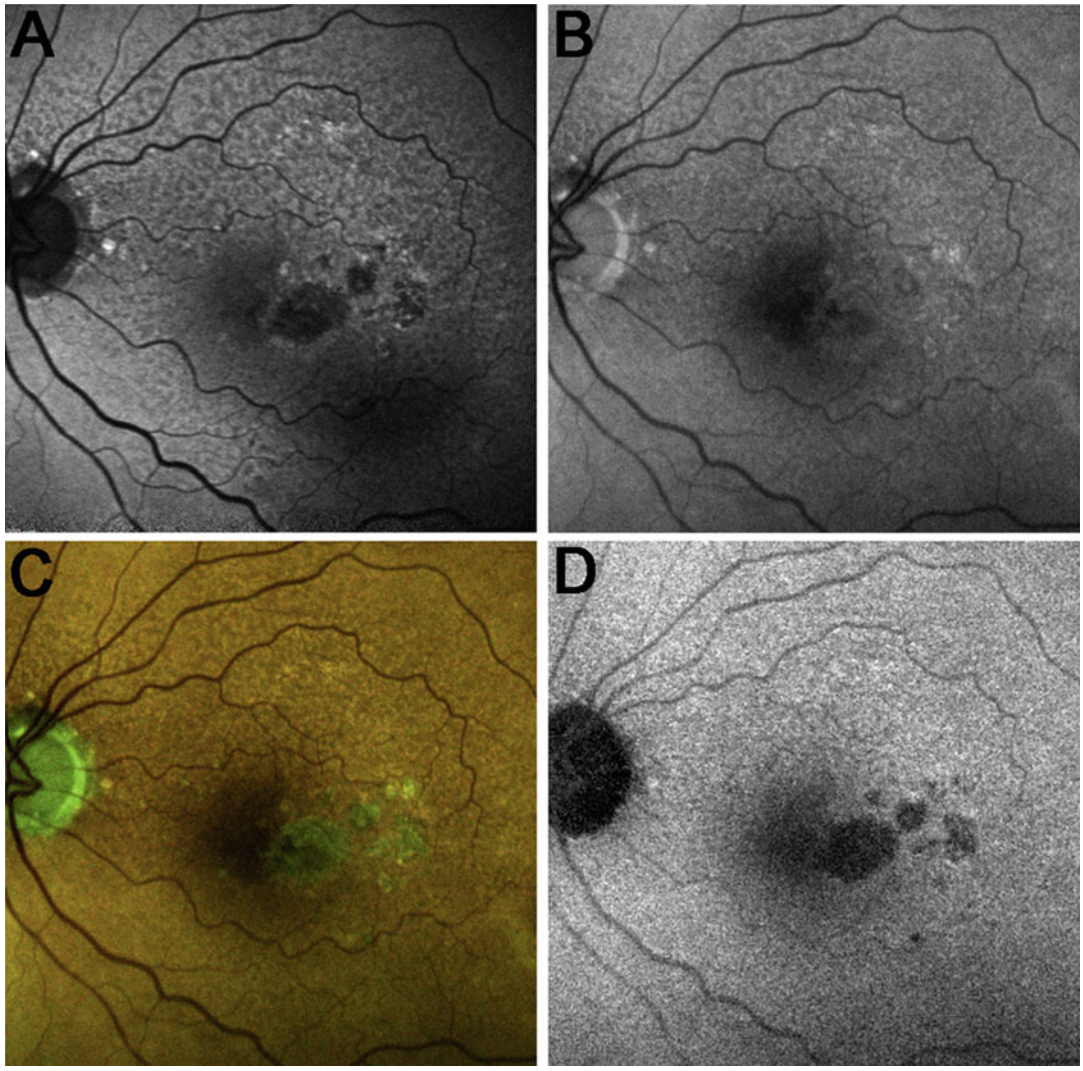

Fig. 2.5 Fundus autofluorescence images from an eye with geographic atrophy secondary to age-related macular degeneration. The 488 nm fundus autofluorescence (FAF) image (**a**) shows well demarcated areas of atrophy that are not visible in the 450 nm FAF (**b**). The color FAF (**c**) shows that in these areas the green emission component (probably due to subretinal deposits) is still present while the red emission component (isolated in **d**) is absent in atrophic regions (due to reduction/absence of lipofucsin)

fundus [73]. Normative studies validated this modality and reported that qAF intensity increases with age, and also vary with sex (higher in women) and ethnicity (higher in whites and Hispanic) [71, 72]. Of note, foveal and perifoveal qAF values are inversely correlated with macular pigment measurements [71, 72]. Obtaining high quality, reliable qAF images does require careful attention to technical details such as uniform illumination, adequate bleaching, optimal focus, and central alignment of the camera with the pupil [73–75].

qAF techniques may have important techniques in inherited retinal diseases, many of which (Stargardt's pattern dystrophies, Best disease) feature accumulations of lipofuscin, and in some cases may be confused with AMD [76–78]. In addition, qAF is being studied in the

setting of AMD, and qAF findings are being correlated to functional measurements (e.g., from electrophysiology and microperimetry) [79]. Large, longitudinal studies are still needed.

2.3.5 Fluorescence Lifetime Imaging Ophthalmoscopy

Fluorescence lifetime imaging ophthalmoscopy (FLIO) uses a blue laser light impulse to excite retinal fluorophores and measure their time span of emission, which is independent from the signal intensity. This parameter is specific for each molecule, depending on its structure and interactions with the local metabolic environment [70]. The latter can change very early during degenerative processes, revealing information about the integrity of RPE and photoreceptors before these changes can be seen by standard imaging modalities [80, 81]. In AMD, fluorescence lifetimes are prolonged compared to healthy subjects [82, 83]. In GA, areas of complete outer retinal and RPE atrophy (cRORA) have longer lifetimes compared to areas where there are surviving photoreceptors segments. This is probably related to fluorophore emission from the connective tissue components and the underlying choroid.

This is a relatively innovative field and more studies assessing metabolic alterations in the pathological retina are required and FLIO can help in supporting this analysis, including in dry AMD.

2.4 Dye-Based Angiography

Dye-based angiography of the retinal fundus consists of two main methodologies according to the type of exogenous fluorphore injected intravenously in the patient for the examination: fluorescein and/or indocyanine green. These fluorophores absorb and emit light at specific wavelengths that can be detected by the camera systems using distinct filters. Several clinical studies have validated the use of SLO systems and flash fundus camera-based systems in both neovascular and dry AMD. Fluorescein angiography and indocyanine green angiography may be performed separately or in combination depending on the diagnostic concern [46].

2.4.1 Fluorescein Angiography

Over the past decades, the diagnosis and grading of MNV were based on fluorescein angiography [84, 85]. It requires the intravenous injection of fluorescein, an organic molecule that shows emits fluorescence when exposed to short-wavelength light (465–490 nm). FA aids in the characterization of numerous retinal abnormalities, such as drusen, vascular alterations, and neovessels. FA is better used to visualize retinal vascularization as the melanin in the RPE absorbs both the exciting and the emitted light on FA. However, wherever the RPE is absent or shows less pigmentation, the CC and choroidal vessels may be seen.

Drusen can be easily visualized by FA but often require the complementary acquisition of other imaging modalities (such as OCT) to distinguish the subtype.

In general, staining properties of soft drusen on FA vary depending on the status of the overlying RPE and the quality of their content [19]. For this reason, they could range from hyper- to hypofluorescent, particularly in the early phases of the angiogram. Given their cross-sectional triangular shape, cuticular drusen have a significant RPE attenuation at the apex and compacting of RPE at the base. This leads to an inverse pattern of presentation between FA and FAF: in FA cuticular drusen show a pinpoint hyperfluorescence centrally ("starry sky" or "milky way" pattern), while in FAF images the apices are hypo-autofluorescent. SDD are hard to visualize on fluorescein angiography, showing absent or minimal fluorescence [86].

The guidelines for the acquisition of FA and the criteria for the identification of MNV secondary to AMD on FA were systematically defined in 1991 with the Macular Photocoagulation Study [84] that distinguished between classic and occult neovascularization. Shortly thereafter another type of neovascularization was identified as a

neovascular process starting from the retinal vasculature and characterized by retinal–retinal or retinal–choroidal anastomosis. The characteristics of each subtypes became more clear with the advent of depth-resolved imaging (such as OCT), leading to a more "modern" classification: type 1 (former "occult") MNV, type 2 ("former" classic) MNV, and type 3 (former "retinal angiomatous proliferation") MNV [3, 87, 88].

Type 2MNVs occupy the subretinal space and generally correspond to classic MNV on FA. Classic MNV is characterized by an area of bright, well-demarcated hyper-fluorescence evident in the early phases of the angiogram. In later phases, progressive leakage and pooling of dye in the overlying subsensory retinal space leads to obscuration of the boundaries of the MNV (Figs. 2.1 and 2.6) [84, 89].

Type 1 MNVs occupy the sub-RPE space and generally correspond to occult CNV on FA. Occult CNV is characterized by areas of irregular elevation of the RPE (fibrovascular PEDs) that may not be as well-demarcated or as bright as areas of classic MNV in the transit phase of the angiogram. Within 1–2 min after fluorescein injection, an area of stippled hyperfluorescence is usually apparent. By 10 min after injection, there is persistent fluorescein staining or leakage within a sensory retinal detachment overlying this area [84, 89]. The exact boundaries of fibrovascular PEDs can be determined only when fluorescence sharply outlines the elevated RPE, although frequently,

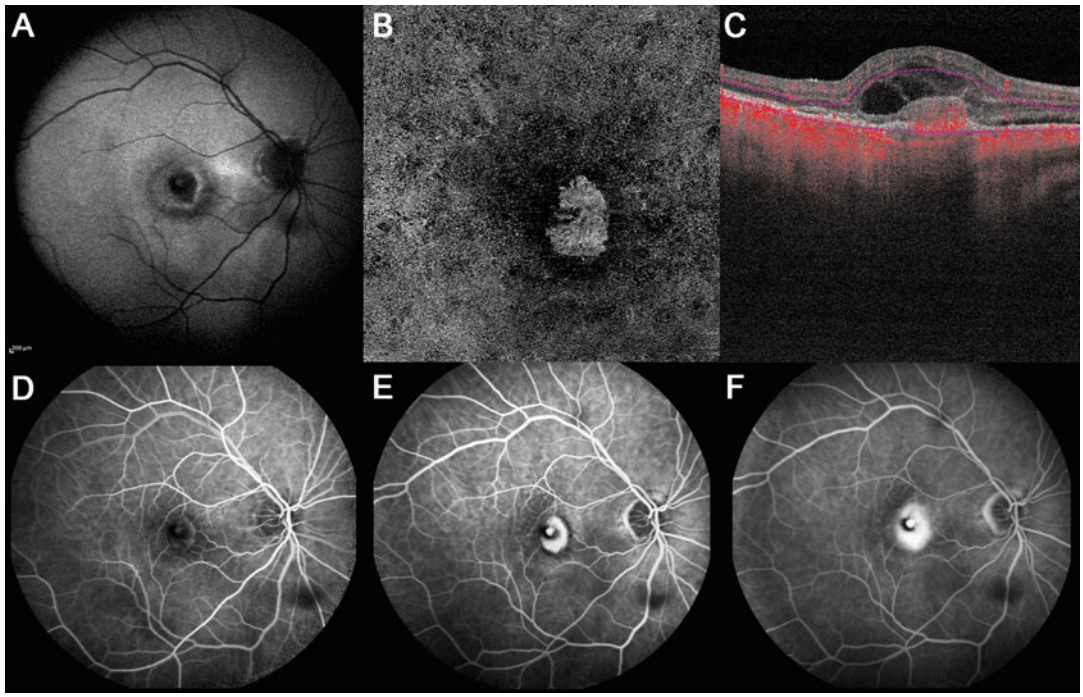

Fig. 2.6 Multimodal imaging of a patient with type 2 macular neovascularization secondary to age-related macular degeneration. Short-wavelength autofluorescence (**a**) shows a hypoautofluorescent area due to blockage by hemorrhage and the neovascular lesion which is positioned above the retinal pigment epithelium (as seen on the optical coherence tomography [OCT] B-scan (**c**)) On *en face* OCT angiography (**b**), the network of vessels is clearly visible and surrounded by a ring of choriocapillaris flow attenuation. The same MNV network is visible by fluorescein angiography, especially during the early (**d**) and late transit phases (**e**). The leakage of dye in the late phase (**f**) makes it more difficult to distinguish the borders of the lesion

the intensity of fluorescence at the boundary of the elevated RPE is quite irregular, with some areas fading relative to the fluorescence of the remaining areas of elevated RPE, making it difficult to distinguish the boundaries of fading fluorescence of the occult MNV from the fading fluorescence of the surrounding RPE. Furthermore, the borders of elevated RPE often slope gradually downward to surrounding flat RPE so that the demarcation between elevated RPE and flat RPE cannot be determined with certainty. Fibrovascular PEDs should not be confused with typical, classic serous detachments of the RPE [90, 91] In the latter, there is usually a uniform, smooth elevation of the RPE with early, sharply demarcated, fairly uniform hyperfluorescence that persists in the late phase of the angiogram [90, 91].

Type 3 MNV may be more difficult to distinguish by FA alone. In the early phases of the angiogram, it shows a leakage often in close proximity to retinal vessels that then becomes intense in late phases, often with cystoid macular edema. Sometimes, in the very early phases it is possible to visualize the retinal–retinal anastomoses. Nevertheless, to reach a sufficient level of confidence for the diagnosis of this type of MNV, ICGA, and/or OCT are often required [3, 89, 92, 93].

The distinction of the specific forms of neovascular AMD is important because some of them show a more severe progression of the disease, critically influencing patient prognostication and the decision-making process for treatment. For instance, retinal angiomatous proliferation (RAP) can present with intraretinal hemorrhage, lipid exudates, and edema in the retinal layers [89, 94]. Furthermore, it is the one with the highest rate of progression to atrophy, with poorer visual outcomes over time [95].

It should be noted that many MNV lesions can feature mixtures of these MNV subtypes that can result in peculiar phenotypeson FA [89].

Other angiographic findings associated with MNV may interfere with the visualization of the lesion boundaries: (1) hemorrhages, hyperplastic pigment, or fibrous tissue contiguous with the MNV may obscure the normal choroidal fluorescence; (2) a serous PED cause an early bright uniform hyperfluorescence that may obscure the fluorescence from MNV. The presence of any of these features can make it impossible to accurately determine the full extent of the MNV [84].

FA can be used for the imaging of GA lesions and is often included in clinical trials in order to rule out the presence of MNV [96, 97]. The presence of leakage associated with MNV may blur the edges of the GA lesion [98, 99] (Fig. 2.7).

Drawbacks of the procedure are its invasiveness, the relatively long time required for capturing the late-phases and the discomfort of patients. Other less invasive methodologies may be preferable alternatives for the differential diagnosis of GA. Furthermore, the risk of severe allergic reaction to intravenous injection of the dye should always be considered.

2.4.2 Indocyanine Green Angiography

Indocyanine green angiography (ICGA) utilizes near-infrared fundus illumination that allows better visualization of deeper structures (e.g., choroid). As this molecule has a higher affinity with plasma proteins than fluorescein, it does not leak from the tiny capillaries in the normal CC; hence, it improves the visualization of the deeper vessels of the choroid [100]. ICGA can be useful for identification of type 3 MNV, revealing a hyperfluorescent spot corresponding to the early angiomatous lesion, which over time may extend from the deep capillary plexus, toward the choroid [100].

ICGA allowed the initial understanding of another form of neovascularization otherwise difficult to recognize by FA alone: the aneurysmal type 1 neovascularization (or polypoidal choroidal vasculopathy) (PCV) [92]. These terms describe the occurrence of aneurysmal lesions that develops from type 1 neovascular networks.

Taking advantage of this better visualization of the choroidal vessels, in 1992, Spaide et al. described PCV as a hyperfluorescent vascular network that forms a “plaque,” masking the

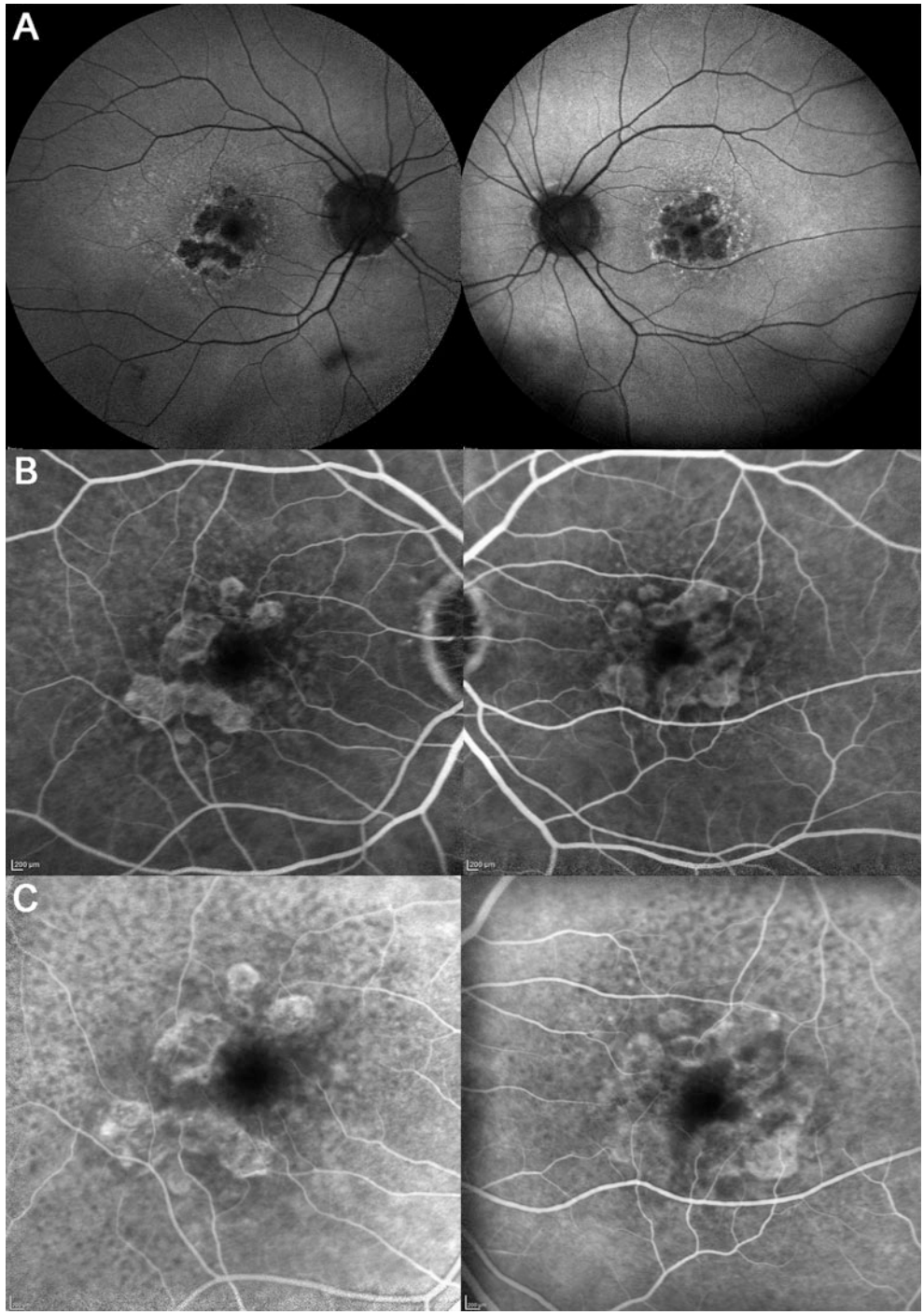

Fig. 2.7 Short-wavelength fundus autofluorescence (**a**) and fluorescein angiography (**b**, **c**) of a patient with bilateral geographic atrophy secondary to age-related macular degeneration. The borders of the lesions are clearly visible during the early phases of the angiogram (**b**) but become less well-demarcated during the late phases (**c**) because of dye leakage and staining

underlying CC and polyps themselves. The latter are evident as hyperfluorescent structures in the early phases of the ICGA, since they subsequently stain and leak from their walls [101].

Only after the introduction of OCT, was the actual depth of these lesions definitely determined [60, 88, 102]. Of note, it is still controversial as to whether PCV is a form of AMD or not [92, 103]. Indeed, there are several differences between PCV and AMD. Peculiarities of PCV are: (1) a thicker subfoveal choroid; (2) the relative absence of classical, and when drusen are present, have an unusual shape [104]; (3) it is more prevalent in African populations (in whom other forms of AMD-related MNVs are uncommon); (4) patients are usually younger; and (5) the development of polypoidal lesions.

ICGA can also aid in the discrimination of atrophic lesions of different origins. For instance, in late-onset Stargardt disease, atrophic areas are not stained by the dye ("dark atrophy"), whereas in AMD, a late staining of the lesions usually occurs [105]. The interest toward the choroid; involvement in the pathogenesis and progression of AMD is particularly high, hence its imaging can be a valuable tool to study and assess it accurately [105–107]. ICGA is an invasive method with the same limitations as FA with regards to imaging time and the risk of allergic reactions.

2.5 Widefield Imaging

Compared to other conventional imaging modalities, widefield imaging can visualize a larger retinal field. The field of view may be extended to >100° using internal or external lenses. Nevertheless, a wider view corresponds to lower resolution and contrast. The SLO modality drives a big proportion of widefield imaging machines, allowing the capture of reflectance images, FAF, or FA and ICGA on the same device. These devices do not use white light, but a mix of discrete laser sources, which are then combined, giving a "false color" image.

A system equipped with an internal ellipsoid mirror (Optos devices; Optos, Dunfermline, UK) can achieve up to a 200° field of view, which covers >80% of the ocular fundus. However, the use of the ellipsoid mirror creates distortion in the periphery of the acquisition; furthermore, the view may be vertically limited by lid and eyelash artifacts [108].

Alternatively, a contact lens may be implemented on an SLO machine in order to achieve a field of view of up to 150° [109]. The use of a contact lens requires a trained operator and can be particularly influenced by the presence of lens opacities [109]. Recently, an ultra-widefield confocal system providing a 105° of view with a noncontact lens attached to the camera has been introduced (Heidelber Engineering, Heidelberg, Germany) [110]. The smaller field of view allows higher contrast without lid and eyelash artifact [110].

Finally, a new color fundus camera with widefield acquisition has become available. This machine (Zeiss Clarus 500; Carl Zeiss Meditec, Dublin, CA) offers the advantages of providing a "true color" image of the fundus with a field of view of 133° in one single image and up to 267° by montage of six pictures. Features graded on standard color photos and widefield image can yield similar findings [111]. Widefield imaging introduced the unprecedented possibility to study, document, and follow the peripheral anomalies associated with AMD [112]. These abnormalities have been noted in >70% of eyes with AMD and include a variety of features such as peripheral drusen, RPE depigmentation, peripheral reticular pigmentary degeneration (PRPD), and/or atrophic patches (Fig. 2.8). It has been suggested that some of these peripheral features may be associated with a worse prognosis (such as PRPD [113, 114]). The natural history of these peripheral lesions and the influence they have on the natural course of the disease require further investigation [115, 116].

2.6 Optical Coherence Tomography

Over the last two decades, the availability of OCT has dramatically transformed ophthalmology,

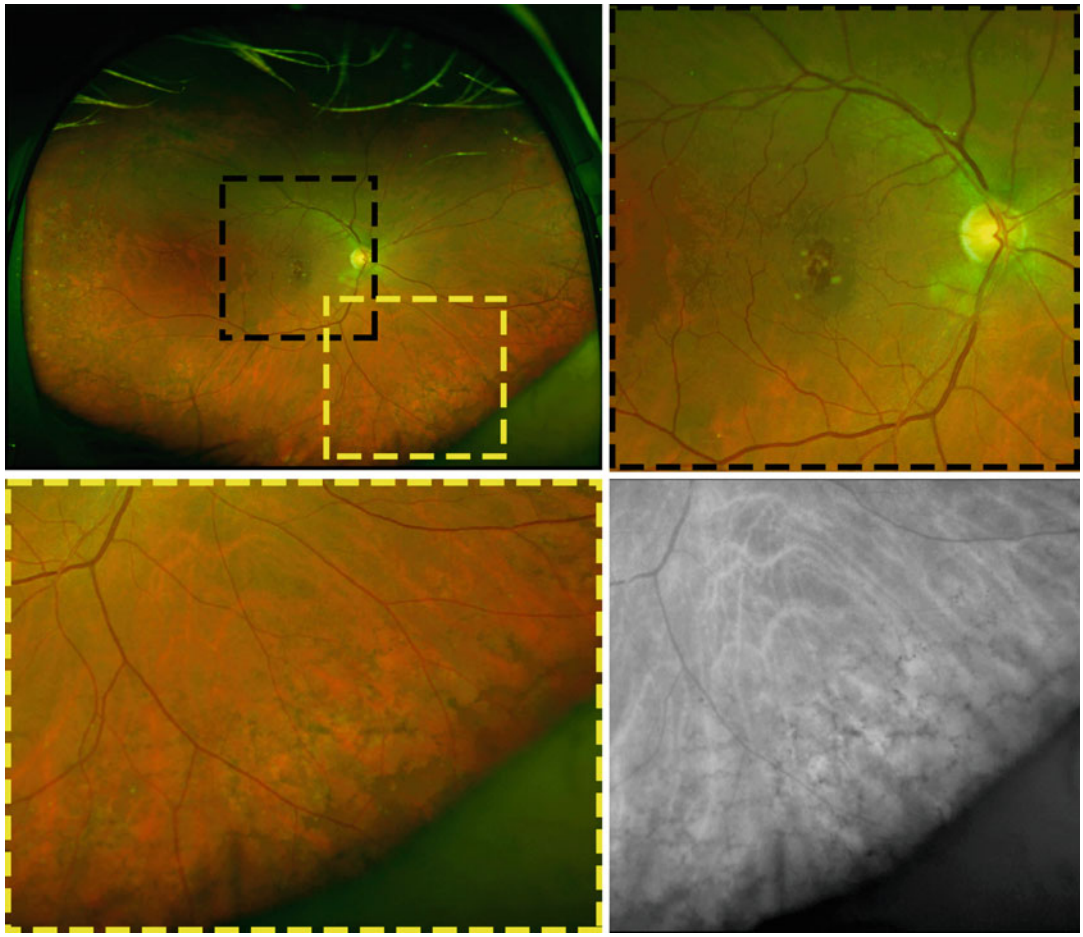

Fig. 2.8 Widefield fundus image (top left) of a patient with dry age-related macular degeneration. The presence of lid artifacts limits the view of the superior field. A magnification of the central field (black box inset on top left → top right) allows better visualization of the drusen in the macular area. Peripheral alterations such as drusen, retinal pigment epithelium depigmentation, and peripheral reticular pigmentary degeneration (PRPD) can be easily seen. The magnification of the infero-nasal field (yellow box, bottom left) highlights the presence of the PRPD, particularly evident in the infrared reflectance image (bottom right)

especially for retinal disease diagnosis and assessment. OCT uses infrared light (with high penetration properties) to measure different backscatter from biological tissues, yielding micrometer-resolution images [117]. OCT imaging can provide depth resolution inside tissues and characterize its structure based on their degree of reflection/scattering of light. Similar to ultrasound imaging, OCT captures multiple images on an axial plane (A-scan), which, when summed up on the transverse plane, provide cross-sections of the tissue (B-scan). Volumetric information is generated by sequentially acquiring multiple B-scans that are displaced perpendicular to the B-scan image, covering an entire region of the retina [117].

Unlike other imaging modalities, OCT produces in vivo cross-sections and en face images of the retinal and subretinal structures [118].

Three different generations of OCT machines have been brought to the market [119–121]. The first OCT device was based on time-domain (TD) technology, which used a light beam

calibrated on a 840 nm wavelength. This device could acquire 400 A-scans every second, and provide images with an axial resolution up to 10–15 μm. Spectral domain (SD)-OCT was the next generation of devices which were introduced and achieved faster scanning speed (25,000–85,000 A-scans per second) and improved resolution (4–7 μm). Enhanced-depth imaging (EDI) SD-OCT yields a higher penetration power and resolution for the imaging of the choroid [122]. Finally, the introduction of swept source (SS)-OCT provided a greater penetration of the choroid, exploiting a light source with wavelength around ~1050 nm. SS-OCT available devices can capture 100,000 A-scans per second, with an axial resolution of 6–8 μm, and can provide B-scans of >20 mm in length. *En face* OCT imaging is commonly used to examine the macula, providing retinal and choroidal sections on the coronal plane (C-scan), which is aligned with the RPE profile as reference.

Eye-tracking systems use anatomic features to align acquisitions from different sessions (useful for follow-up) and facilitate the acquisition of scans in eyes with poor stability of fixation. A single B-scan may be acquired quickly while a dense raster pattern of line-scans ("volume scan") often requires more time. Nevertheless, volume scans with sufficiently small spacing between consecutive B scans are necessary to elaborate the C-scans, which allow the mapping of the macula and the localization of specific features, such as drusen, reticular pseudodrusen, and pigment migration into the inner retina. In early and intermediate stages of AMD, the high-resolution of the OCT scans provides an excellent visualization of the morphology of drusen and the overlying RPE and neurosensory retina [123].

Small (hard), medium, and large (soft) drusen appear as deposits of hyper-reflective material between the RPE basal lamina and Bruch's membrane (Fig. 2.9) [19].

The coalescence of large drusen may lead to a drusenoid PED. OCT imaging can identify the presence of PED, showing a dissociation between the RPE and the Bruch's membrane [44]. The inner contour of the PED (equivalent to the RPE band) usually appears smooth and undulating. OCT can supply useful information on the dimension of drusen (i.e., height, area, and volume), but also regarding their shape and internal reflectivity, as well as the integrity of the overlying RPE. Several studies have reported that drusen show a dynamic appearance, with their volume increasing and decreasing cyclically [123, 124]. Several prognostic factors associated with drusen could be easily evaluated by OCT. A greater risk of progression to focal atrophy has been associated with (1) greater heights of drusenoid lesions or PED [123]; (2) drusen regression [125]; (3) internal heterogeneous reflectivity or hyporeflective drusen cores (Fig. 2.9) [123, 126]; (4) finally, mineralized drusen with refractile deposits (supposedly calcified or mineralized lipid material), which may be a form of drusen in regression [127]. Cuticular drusen are small drusen that demonstrate a characteristic "sawtooth" pattern on OCT (small, triangle-shaped, hyporeflective inside) [19]. Finally, subretinal drusenoid deposits (which correlate with reticular pseudodrusen on FAF) have been classified using OCT in three different stages: stage 1 shows a wavy or ribbon-like EZ, in stage 2 the EZ deflects inward as a result of the deposit, while stage 3 features the interruption of the EZ and the inward deviation of the external limiting membrane [20].

Several studies have shown that reticular pseudodrusen are associated with a higher risk of developing late AMD [128, 129] and atrophic degeneration of the outer retina. Nevertheless, it is still debated if reticular pseudodrusen may forecast the rate of future growth of the lesions, as their presence usually anticipate where GA would develop and the risk of multifocal lesions [122].

Other AMD-related features that OCT may help to identify in the earlier stages are pigmentary alterations: choroidal hypertransmission (i.e., increased light transmission through the choroid because of the overlaying retinal atrophy) may help identify focal areas of RPE loss or depigmentation [130]; pigment clumping and migration are visualized in OCT as outer retinal hyper-reflective foci. The latter have been related

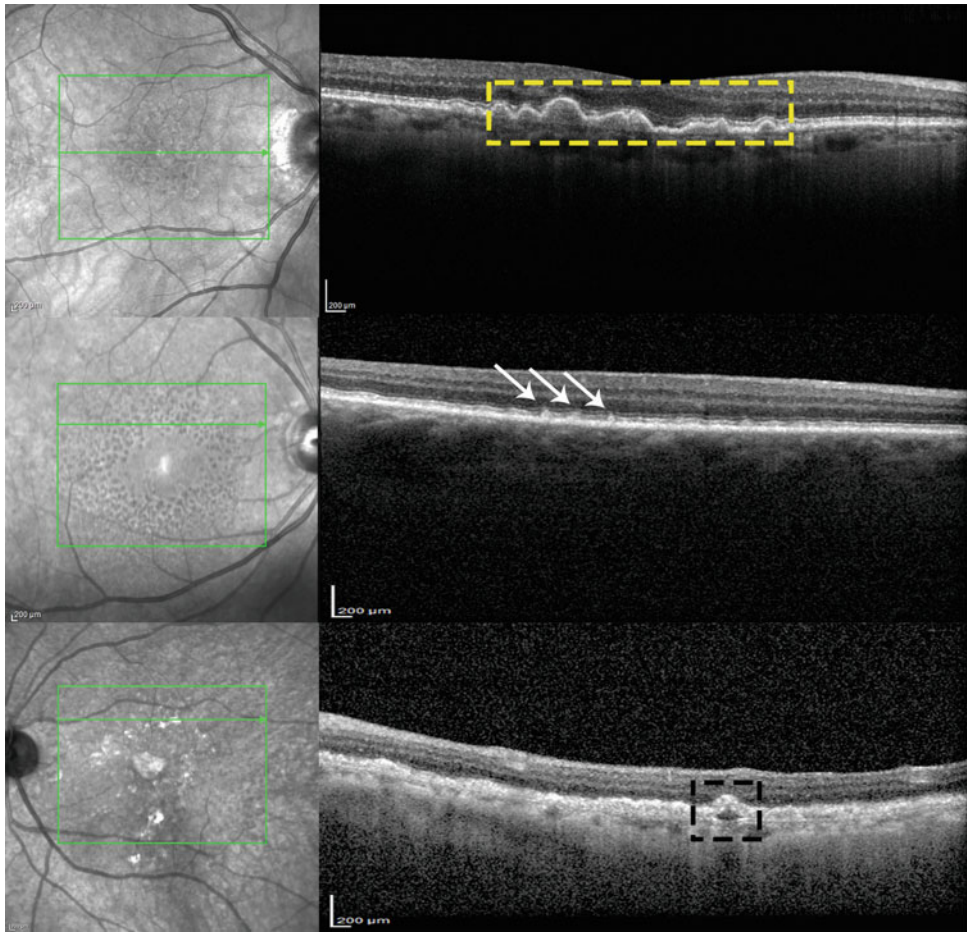

Fig. 2.9 Infrared reflectance (IR) and optical coherence tomography B-scans of three patients with dry age-related macular degeneration. The first subject (first row) shows soft confluent drusen (yellow box) close to the foveal center; the second patient (second row) shows a ring-like pattern of reticular pseudodrusen on the IR image with corresponding subretinal drusenoid deposits (white arrows) on the OCT B-scan. The third patient (bottom row) has focal areas of geographic atrophy associated with hyporeflective drusen (black box)

to RPE atrophic degeneration and associated with a higher probability for focal atrophic lesions to develop and progress [123, 129, 131, 132].

The clinical relevance of OCT is also important in the later stages of AMD (both GA and MNV), and its structural findings are often included in clinical trials as primary and/or secondary endpoints for treatment success.

OCT can identify exudative AMD at an early stage. Type 1 MNV is localized under the RPE, constituting a vascularized fibrovascular or serous PED. Serous PEDs are usually smooth regular dome-shaped hyporeflective RPE elevations. Fibrovascular PEDs are filled with a medium-to-high reflective material organized in multiple layers that are separated by hyporeflective spaces (Fig. 2.4).

Active type 1 MNV is often accompanied by subretinal fluid (SRF) that accumulates between the retina and the RPE and appears hyporeflective. Intraretinal fluid (IRF) is less common for type 1 MNV (generally present with older, more chronic lesions) and appears as round, hyporeflective, cystoid spaces within the retinal layers. Not all these spaces are indicative of exudation, and persistent cystoid spaces

despite therapy, particularly with less associated retinal thickening, may be a feature of retinal degeneration [3, 89].

Type 2 MNV is localized in the subretinal space, directly above the RPE (Figs. 2.1 and 2.6). It is frequently associated with retinal thickening, SRF, IRF, and PED [133].

Type 3 MNV is typically preceded by the migration of RPE cells (intraretinal hyperreflective foci) into the retina. These RPE cells may locally secrete VEGF and promote the development of the NV lesion at the level of the deep capillary plexus. The NV lesion may then grow downward and reach the sub-RPE space through a gap in the RPE monolayer that is commonly present. OCT features that aid in the identification of Type 3 NV include: (1) a gently sloping dome-shaped or trapezoid-shaped PED without an obvious peak and with a "flap" sign; (2) a focal funnel-shaped defect in the RPE, called the "kissing sign"; (3) presence of IRF and often (but not always) absence of SRF [93, 134] (Fig. 2.10).

In aneurysmal type 1 neovascularization (or PCV), the branching vascular network appears as a fibrovascular PED, while the aneurysmal lesions themselves appear as a PED with sharper bumps, often correlating with an internal rounded hyporeflective area (representing the polyp lumen) and exudative findings [92, 135].

To date, OCT is the gold-standard imaging technique for assessing exudative AMD over the long term and has largely replaced CFP and FA for monitoring the activity of the disease thanks to its higher sensitivity. Serial consecutive assessments of macular thickness and morphology allow the evaluation of the response to treatment. It is particularly valuable in case of individualized or evaluation-based, as-needed therapy (Pro Re Nata, PRN), which is one of the two treatment regimens commonly employed in practice. The presence of any fluid generally guides the decision to retreat patients [96, 136]. Structure–function correlation has identified OCT biomarkers that are commonly associated with reduced vision: IRF at baseline and persistent cystoid spaces at the end of the loading dose (independently from the agent and regimen chosen) [137]. Whenever IRF is present initially, best corrected visual acuity (BCVA) and the gain in BCVA may be reduced compared to eyes with only SRF [137].

OCT is also currently used for a precise assessment of GA. Its depth resolution characteristics yield precise measurements and evaluation of the single layers of both the retina and choroid [138], and may facilitate the detection of early or nascent atrophy before it may be detected by CFP or FAF.

Recently, an OCT-based classification of macular atrophy was proposed by a consensus of retinal specialists and image reading center experts through the Classification of Atrophy Meetings (CAM) program [130]. Four terms

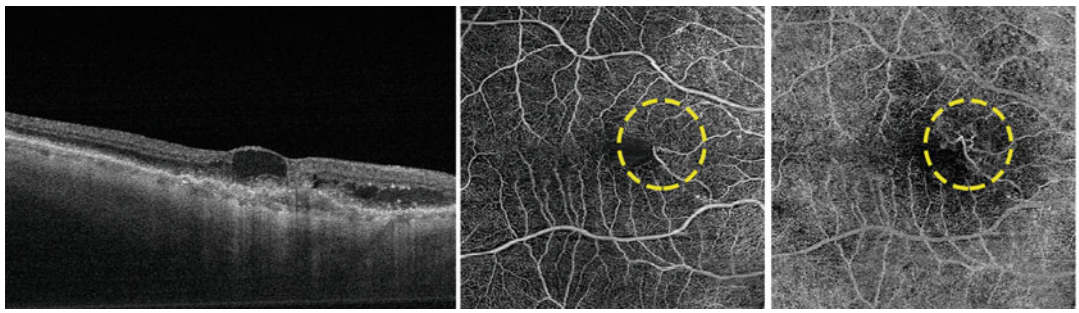

Fig. 2.10 Optical coherence tomography (OCT) and OCT angiography of type 3 macular neovascularization. The B-scan (left) shows a trapezoid-shaped pigment epithelial detachment with the typical "kissing sign" and the presence of intraretinal fluid. On OCT angiography, this type of neovascularization can be visualized as a discrete high flow linear structure (yellow dotted circle) extending from the middle retinal layers (middle) into the deep retina (right)

were proposed to describe atrophy in the setting of AMD: "complete RPE and outer retina atrophy (cRORA)", "incomplete RPE and outer retinal atrophy (iRORA)", "complete outer retinal atrophy (cORA)", and "incomplete outer retinal atrophy (iORA)".

GA was defined to be a subcategory of cRORA with no MNV, whereas cRORA is identified as a condition of macular atrophy with or without MNV. Nascent GA [139] is considered as a subcategory of iRORA with no MNV. The cRORA is defined by the concomitant presence of three specific OCT criteria: (1) an area of light hypertransmission into the choroid with a minimum diameter of 250 μm; (2) a region of attenuated or absent RPE, 250 μm in minimum diameter; and (3) signs of degeneration of photoreceptors (absence of the interdigitation zone, external limiting membrane, and EZ and reduction of the thickness of the external nuclear layer), without a scrolled RPE or other evidence of an RPE rip. In ambiguous cases, it has been advised that OCT evaluation should be assisted by other imaging technologies.

OCT is valuable not only for the diagnosis, but also for assessing the progression of GA: when the lesion borders present with irregular RPE elevations [140], an evident separation between the RPE and the Bruch's membrane [140], and/or a thickening of the inner nuclear layer thickness [141], the GA is more likely to grow faster than lesions with smooth edges. Furthermore, an outer retinal thinning often appears at the border of the lesions before the atrophy progresses [142].

Another OCT finding that may be observed in eyes with RPE loss (including eyed with GA) is outer retinal tubulation (ORT). OCT B-scans detect ORTs as round-shaped structures in the outer nuclear layer. Using the *en face* OCT, it is often evident that these structures are connected in a multiple branching morphology [142–144]. ORTs show a hyporeflective lumen surrounded by a hyper-reflective ring that is the outer limiting membrane. It is still questioned if ORTs have clinically important prognostic value [122, 145, 146].

The rising availability of EDISD-OCT and SS-OCT has facilitated evaluation of the choroid in various disorders including AMD. It has been speculated that a drop in the perfusion of the choroid can result in ischemia of the external retina, which is considered an important pathogenic trigger in the pathogenesis of both non-neovascular and neovascular AMD [146–148]. Some studies have associated the thickness of the choroid with the AMD condition: the choroid tends to be thinner as the disease progresses, especially in dry AMD [149, 150, 151]. However, this is still debated as other reports did not confirm these findings [152, 153].

2.7 Optical Coherence Tomography Angiography

Optical coherence tomography angiography (OCTA) is another promising and rapidly evolving technology that can provide visualization of flow in the retinal microcirculation in a depth-resolved fashion [154–156]. The relatively quick acquisition time, lack of need of intravenous dye, and the high-resolution and contrast of the resultant images are major advantages of OCTA.

This technology is based on the principle that the flow in the retinal blood vessels is the main source of motion in the posterior segment of the eye. Thus, by acquiring repeated B-scans at the same position, differences in phase and amplitude of the reflected light signals can be used to identify regions in B-scans where presumed flow is present.

The image resulting from the pixel-by-pixel comparison of two or more repeated B-scan (automatically done by different algorithms in different machines) at the same position is displayed as a motion contrast image. OCTA represents the volumetric reconstruction of a dense raster of repeated consecutive B-scans, which allows the depth-resolved *en face* visualization of the retinal and choroidal microvasculature. Unlike FA, OCTA allows the capillaries in different retinal layers to be isolated and visualized. In this way, a precise correlation between vascular, structural, and functional

changes can be performed in vivo in both cross-sectional and longitudinal fashions.

The first OCTA system was implemented on an SD-OCT platform. Recently, the implementation of this system on SS-OCT with longer (1050 nm) wavelengths has facilitated better assessment of the CC and choroid (Fig. 2.11).

Choriocapillaris alterations have been observed throughout all phases of non-neovascular AMD. In early and intermediate AMD, OCTA has identified reduced CC flow signal under and around drusen, confirming previous histological studies [157–159]. These findings could be indicative of true nonperfusion due to CC impairment or may simply reflect a reduction of blood flow velocity below the detectable threshold of current OCTA technology. Regardless, both scenarios may be associated with hypoxia of the RPE and photoreceptors, with consequent derangement of the local metabolic environment. Eyes with reticular pseudodrusen seem to have even more extensive impairment of the CC as well as a reduced choroidal thickness, particularly in the extrafoveal quadrants [160, 161].

This CC impairment in the earlier stages of AMD seems also to correlate with photoreceptor function, since a significant association has been found between the absence of flow signal and electroretinogram implicit times [162]. In intermediate AMD, but not in early AMD, OCTA has also shown alterations in the superficial and deep

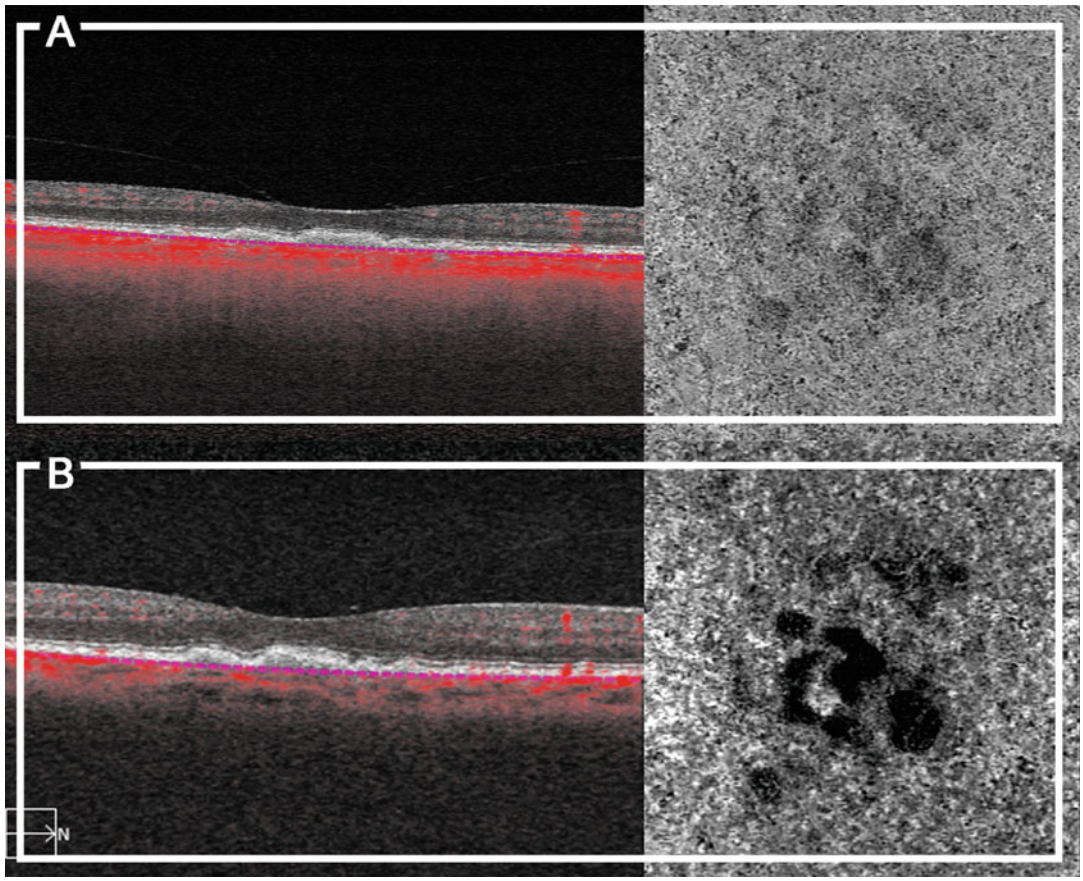

Fig. 2.11 Swept-source (**a**) and spectral domain (**b**) optical coherence tomography angiography of a patient with drusen. The higher penetration of the longer wavelength used by the swept-source systems allows a clearer visualization of the choriocapillaris (right) under the drusen

retinal plexuses, which also seem to correlate with choroidal thickness reduction [163].

In GA, the CC is highly impaired in within these advanced atrophic lesions, even though some residue of flow can be still detected near the border of these lesions. However, the CC immediately surrounding the GA lesion (under apparently intact RPE) can show substantial impairment (Fig. 2.12) [164, 165].

Recently, a report on OCTA showed a significant relationship between areas of nascent GA and CC alterations [166].

It is still debated whether the RPE or the CC disruption occurs first in AMD with evidence

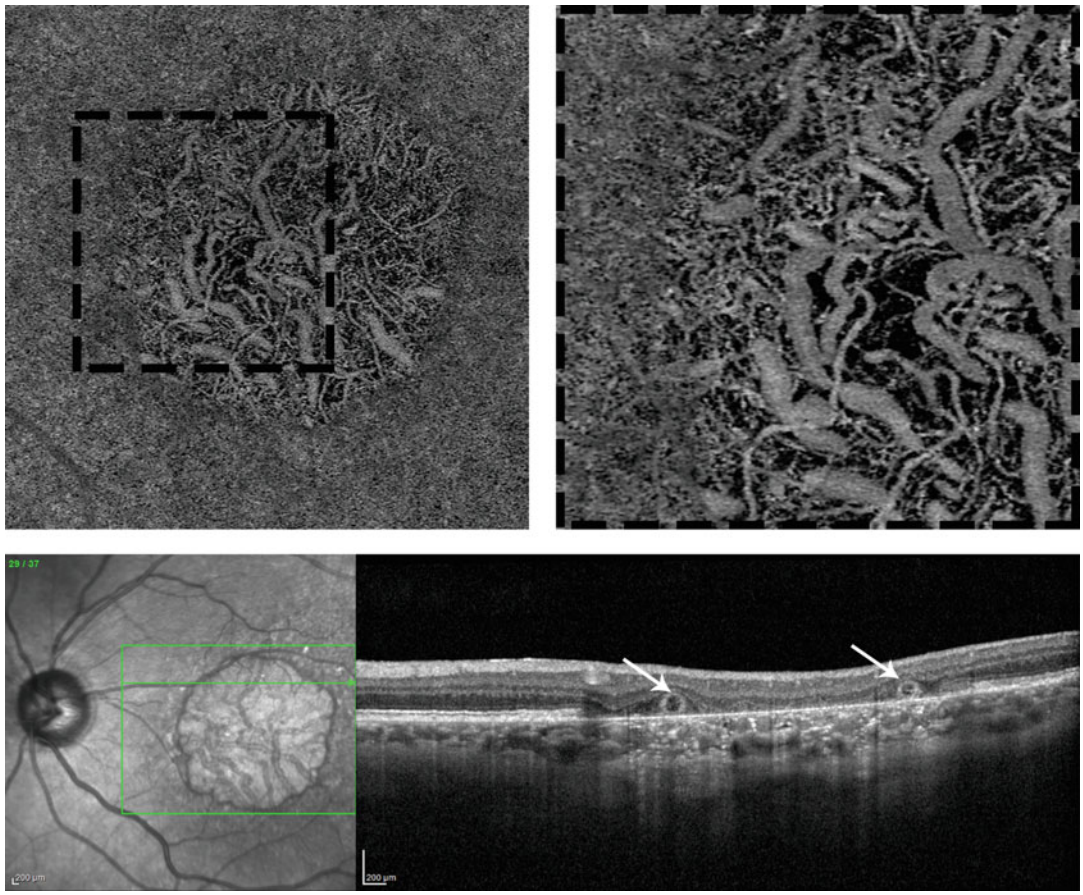

Fig. 2.12 Multimodal imaging of a patient with geographic atrophy secondary to age-related macular degeneration. Optical coherence tomography (OCT) angiography (first row) shows evidence of flow in large choroidal vessels within the atrophic region where the choriocapillaris (CC) is significantly impaired/atrophic and the retinal pigment epithelium (RPE) is absent. The CC also appears to be impaired near the margin of the atrophy (black dotted box). The near infrared image (second row, left) shows the exact boundaries of the lesion. In the OCT B-scan (second row, right), evidence of complete RPE and photoreceptor atrophy with choroidal hypertransmission, attenuation of the RPE band, and thinning of the overlying outer retina can be seen. Areas of outer retinal tubulations (white arrows) can also be observed

pointing in both directions [158, 166–169]. Recent in vivo studies using OCTA seemed to support the hypothesis that CC loss may precede RPE degeneration as microvascular changes occur even under areas of intact RPE. Nevertheless, it is still possible that current imaging methodologies are not sensitive enough to detect the earliest dysfunction of the RPE. Furthermore, the reduced production of trophic factors from the damaged or absent adjacent RPE may also contribute to CC impairment in regions surrounding GA lesions [158, 167].

The use of OCTA has also been investigated for detecting "silent" type 1 MNV in otherwise asymptomatic intermediate AMD patients. A case series has estimated this occurrence in around 30% of all eyes with intermediate AMD [170]. OCTA may be used for diagnosing different subtypes of MNV, allowing a direct correlation with structural OCT and thereby aiding in the diagnosis and classification of the neovascular lesions [171]. Type 1 MNV is usually displayed as a network of vessels between the RPE and the Bruch's membrane, often in the setting of a fibrovascular PED as visualized on the OCT (Fig. 2.4) [172]. Conversely, Type 2 MNV is displayed as a vascular network in the avascular subretinal space (Fig. 2.6) [173]. In both these MNV types, it is often possible to see on OCTA the feeding trunk vessels: generally large vessel from which smaller vessels derive, forming anastomotic connections inside and at the borders of the lesions [174–176]. Furthermore, there may be drop out of the CC surrounding areas of MNV [168] confirming previous histological studies [177].

Type 3 MNV, on the other hand, can be visualized as a discrete high flow linear structure extending from the middle retinal layers into the deep retina and occasionally through the RPE (Fig. 2.9). OCTA findings may be difficult to see in the earliest stages of Type 3 MNV, and thus structural OCT remains important for diagnosis. When type 3 MNV progresses, vessel branches form anastomotic connections within the deep capillary plexus, extending downward to the external retina and subretinal and sub-RPE spaces [175].

Current studies using OCTA in neovascular AMD are aimed at defining imaging features that could aid clinicians to distinguish between active and inactive MNV [178]. Different authors advocate that some OCTA findings (e.g., dark haloes surrounding the lesions and tiny vessels at the MNV edges) may correlate with activity, whereas bigger "dead tree"-shaped vessels and a lack of fine vessels branches may correlate with quiescent lesions [171]. The reliability of identifying these features remains to be established. Nevertheless, a lesion defined as "active" may not always implicate poor visual acuity while an "inactive" fibrovascular scar may be associated with poor visual acuity. These observations may eventually assist in defining the optimal endpoint or outcome following anti-VEGF therapy MNV, though prospective longitudinal studies will be essential [156].

A challenge for evaluating the OCTA of eyes with suspected MNV is to avoid misinterpretation due to various artifacts, some of which include: (1) areas of atrophy that may reveal flow in deeper choroidal vessels that could be confused for neovascularization; (2) projection artifacts from retinal vessels projecting onto elevated hyperreflective structures such as serous PED, drusen, drusenoid PED, and pigmented scars thereby simulating neovascularization [177]; (3) particularly for type 3 MNV, superficial vessels may be projected on the highly reflective PED, simulating a MNV [179, 180]; and finally (4) hemorrhages or other features of exudation may obscure the flow signal, preventing visualization of the MNV [181]. Use of projection removal software as well as a systematic review of the OCTA with simultaneous viewing of the corresponding structural OCT *en face* image as well as the B-scans with flow overlay can prevent misinterpretation of these artifacts.

Various studies have evaluated the sensitivity and specificity of OCTA in identifying MNVs [174, 182], resulting in an overall sensitivity of ~50% and a specificity above 80% [182]. The sensitivity seems to be higher when considering only Type 1 MNV (66.7%), with further increase in detection rate when OCTA is accompanied by structural OCT data (87%) [172, 183].

Current commercial OCTA devices present a small dynamic range for flow velocity, with the

output saturating at low flow rates. The ability to quantifying flow rates could potentially prove to be useful for an accurate identification of MNV and the evaluation of the efficacy of treatments, but such an analysis is not currently available in clinical devices.

OCTA has several limitations that must be taken into consideration when evaluating the images: (1) the absence of signal may not indicate an absence of flow, but only a flow below the threshold of detection; (2) low OCT signal, but above the threshold level may give rise to a decorrelation signal due to noise; and (3) the presence of RPE alterations may preclude a clear visualization of the underlying CC. These issues must be considered when evaluating OCTA images for the presence of CC dropout [158]. Thus, swept-source devices, which use longer wavelength, are less prone to attenuation artifacts and may be more suitable for CC visualization [120, 184–187].

Finally, motion, projection, and segmentation artifacts are further drawback of this imaging methodology. However, more efficient tracking systems and projection removal algorithms as well as deep-learning algorithms for segmentation could potentially overcome these limitations in future [176].

2.8 Adaptive Optics Scanning Laser Ophthalmoscopy

Adaptive optics scanning laser ophthalmoscopy can produce in vivo images of individual cone photoreceptors and images of the RPE mosaic. This technology has a lateral image resolution of 2 μm achieved by compensating for ocular wavefront aberrations. This resolution allows the reproducible visualization of individual cone photoreceptors that may be reliably tracked over time [188–190]. Usually, AOSLO methodology employs along wavelength (e.g., 840 nm) [191]. Media opacities and poor fixation are major obstacles to obtain good quality images as they may cause light scattering and image distortion, respectively [192].

Increasing degrees of severity of AMD lead to increasing photoreceptors loss as demonstrated by the use of AOSLO [193]. There is a slight disruption of the photoreceptor mosaic over small drusen while in presence of soft drusen and/or drusenoid PEDs and/or areas of GA, photoreceptor density is significantly decreased [193]. In patients with GA and drusen, the correlation between AOSLO and other modalities (SD-OCT, SW-FAF, NIR-FAF, and CFP) has shown that the cone mosaic is continuous, with normal intercellular spacing over drusen up to the edge of GA [194]. Nevertheless, the reflectivity of the cones over drusen is often reduced and colocalizes with overlying hyporeflective EZ on OCT [194].

No correlation was found between the AOSLO dark signal and the presence of hyperautofluorescent GA borders in FAF images [195]. The spacing of the cones has a high specificity but not the same sensitivity in measuring the integrity of the mosaic-like structure of photoreceptors and thus cannot be a reliable index of the progression of the disease [194]. Of note, in the presence of RPE or retinal profile alterations (e.g., drusen or GA), the alignment of the cones might change making them appear artificially hyporeflective [194, 196]. These findings do not consistently correlate with histology and OCT studies that report a decrease in the density of photoreceptors over drusen [197, 198]. On the other hand, they correlate well with histology and OCT studies reporting photoreceptor alterations at the edge of GA [51, 195, 199]. Recently, photoreceptor abnormalities were detected in AMD patients in areas of normal SW-FAF [192], which seem to correspond with histologic changes of AMD [52]. Therefore, AOSLO could anticipate the identification of abnormal findings in RPE cells and/or in the overlying photoreceptors before they become visible with SW-FAF, NIR-FAF, or even SD-OCT. These findings may represent features of AMD progression that can be tracked in a quantitative and reproducible fashion.

2.9 Summary

In summary, advances in ocular imaging have significantly enhanced our ability to comprehensively evaluate the eyes of patients with AMD. These imaging approaches can allow early diagnosis of AMD and precise monitoring of its

progression. The various imaging modalities provide complementary information and are optimally used in multimodal approach.

References

1. Holz FG, Sadda SR, Staurenghi G et al (2017) Imaging protocols in clinical studies in advanced age-related macular degeneration: recommendations from classification of atrophy consensus meetings. Ophthalmology 124:464–478. https://doi.org/10.1016/j.ophtha.2016.12.002
2. Garrity ST, Sarraf D, Freund KB, Sadda SR (2018) Multimodal imaging of nonneovascular age-related macular degeneration. Invest Ophthalmol Vis Sci 59: AMD48–AMD64. https://doi.org/10.1167/iovs.18-24158
3. Schmidt-Erfurth U, Chong V, Loewenstein A et al (2014) Guidelines for the management of neovascular age-related macular degeneration by the European Society of Retina Specialists (EURETINA). Br J Ophthalmol 98:1144–1167. https://doi.org/10.1136/bjophthalmol-2014-305702
4. Lim LS, Mitchell P, Seddon JM et al (2012) Age-related macular degeneration. Lancet Lond Engl 379:1728–1738. https://doi.org/10.1016/S0140-6736(12)60282-7
5. Zarbin MA (2004) Current concepts in the pathogenesis of age-related macular degeneration. Arch Ophthalmol Chic Ill 1960 122:598–614. https://doi.org/10.1001/archopht.122.4.598
6. Handa JT (2012) How does the macula protect itself from oxidative stress? Mol Aspects Med 33:418–435. https://doi.org/10.1016/j.mam.2012.03.006
7. Sparrow JR, Ueda K, Zhou J (2012) Complement dysregulation in AMD: RPE-Bruch's membrane-choroid. Mol Aspects Med 33:436–445. https://doi.org/10.1016/j.mam.2012.03.007
8. Ferris FL, Davis MD, Clemons TE et al (2005) A simplified severity scale for age-related macular degeneration: AREDS Report No. 18. Arch Ophthalmol Chic Ill 1960 123:1570–1574. https://doi.org/10.1001/archopht.123.11.1570
9. Wang JJ, Foran S, Smith W, Mitchell P (2003) Risk of age-related macular degeneration in eyes with macular drusen or hyperpigmentation: the Blue Mountains Eye Study cohort. Arch Ophthalmol Chic Ill 1960 121:658–663. https://doi.org/10.1001/archopht.121.5.658
10. Klein R, Klein BEK, Tomany SC et al (2002) Ten-year incidence and progression of age-related maculopathy: the Beaver Dam eye study. Ophthalmology 109:1767–1779
11. van Leeuwen R, Klaver CCW, Vingerling JR et al (2003) The risk and natural course of age-related maculopathy: follow-up at 6 1/2 years in the Rotterdam study. Arch Ophthalmol Chic Ill 1960 121:519–526. https://doi.org/10.1001/archopht.121.4.519
12. Age-Related Eye Disease Study Research Group (2001) The Age-Related Eye Disease Study system for classifying age-related macular degeneration from stereoscopic color fundus photographs: the Age-Related Eye Disease Study Report Number 6. Am J Ophthalmol 132:668–681
13. Jain N, Farsiu S, Khanifar AA et al (2010) Quantitative comparison of drusen segmented on SD-OCT versus drusen delineated on color fundus photographs. Invest Ophthalmol Vis Sci 51:4875–4883. https://doi.org/10.1167/iovs.09-4962
14. Leuschen JN, Schuman SG, Winter KP et al (2013) Spectral-domain optical coherence tomography characteristics of intermediate age-related macular degeneration. Ophthalmology 120:140–150. https://doi.org/10.1016/j.ophtha.2012.07.004
15. Folgar FA, Chow JH, Farsiu S et al (2012) Spatial correlation between hyperpigmentary changes on color fundus photography and hyperreflective foci on SDOCT in intermediate AMD. Invest Ophthalmol Vis Sci 53:4626–4633. https://doi.org/10.1167/iovs.12-9813
16. Abràmoff MD, Garvin MK, Sonka M (2010) Retinal imaging and image analysis. IEEE Rev Biomed Eng 3:169–208. https://doi.org/10.1109/RBME.2010.2084567
17. Bird AC, Bressler NM, Bressler SB et al (1995) An international classification and grading system for age-related maculopathy and age-related macular degeneration. The International ARM Epidemiological Study Group. Surv Ophthalmol 39:367–374
18. Ferris FL, Wilkinson CP, Bird A et al (2013) Clinical classification of age-related macular degeneration. Ophthalmology 120:844–851. https://doi.org/10.1016/j.ophtha.2012.10.036
19. Spaide RF, Curcio CA (2010) Drusen characterization with multimodal imaging. Retina Phila PA 30:1441–1454. https://doi.org/10.1097/IAE.0b013e3181ee5ce8
20. Spaide RF, Ooto S, Curcio CA (2018) Subretinal Drusenoid Deposits AKA Pseudodrusen. Surv Ophthalmol. https://doi.org/10.1016/j.survophthal.2018.05.005
21. Wu Z, Ayton LN, Luu CD et al (2016) Reticular pseudodrusen in intermediate age-related macular degeneration: prevalence, detection, clinical, environmental, and genetic associations. Invest Ophthalmol Vis Sci 57:1310–1316. https://doi.org/10.1167/iovs.15-18682
22. De Bats F, Mathis T, Mauget-Faÿsse M et al (2016) Prevalence of reticular pseudodrusen in age-related macular degeneration using multimodal imaging. Retina Phila PA 36:46–52. https://doi.org/10.1097/IAE.0000000000000648

23. Mokwa NF, Ristau T, Keane PA et al (2013) Grading of age-related macular degeneration: comparison between color fundus photography, fluorescein angiography, and spectral domain optical coherence tomography. J Ophthalmol 2013:385915. https://doi.org/10.1155/2013/385915
24. Tan ACS, Fleckenstein M, Schmitz-Valckenberg S, Holz FG (2016) Clinical application of multicolor imaging technology. Ophthalmol J Int Ophtalmol Int J Ophthalmol Z Augenheilkd 236:8–18. https://doi.org/10.1159/000446857
25. Webb RH, Hughes GW, Delori FC (1987) Confocal scanning laser ophthalmoscope. Appl Opt 26:1492–1499
26. Alten F, Clemens CR, Heiduschka P, Eter N (2014) Characterisation of reticular pseudodrusen and their central target aspect in multi-spectral, confocal scanning laser ophthalmoscopy. Graefes Arch Clin Exp Ophthalmol Albrecht Von Graefes Arch Klin Exp Ophthalmol 252:715–721. https://doi.org/10.1007/s00417-013-2525-y
27. Ben Moussa N, Georges A, Capuano V et al (2015) MultiColor imaging in the evaluation of geographic atrophy due to age-related macular degeneration. Br J Ophthalmol 99:842–847. https://doi.org/10.1136/bjophthalmol-2014-305643
28. Pang CE, Freund KB (2014) Ghost maculopathy: an artifact on near-infrared reflectance and multicolor imaging masquerading as chorioretinal pathology. Am J Ophthalmol 158:171–178.e2. https://doi.org/10.1016/j.ajo.2014.03.003
29. Lei J, Al-Sheikh M, Shi Y et al (2017) Reliability of confocal white-light fundus imaging for measurement of retina pigment epithelial atrophy in age-related macular degeneration. Retina Phila PA. https://doi.org/10.1097/IAE.0000000000001949
30. Elsner AE, Burns SA, Weiter JJ, Delori FC (1996) Infrared imaging of sub-retinal structures in the human ocular fundus. Vision Res 36:191–205
31. Suzuki M, Sato T, Spaide RF (2014) Pseudodrusen subtypes as delineated by multimodal imaging of the fundus. Am J Ophthalmol 157:1005–1012. https://doi.org/10.1016/j.ajo.2014.01.025
32. Manivannan A, Kirkpatrick JN, Sharp PF, Forrester JV (1994) Clinical investigation of an infrared digital scanning laser ophthalmoscope. Br J Ophthalmol 78:84–90
33. Diniz B, Ribeiro RM, Rodger DC et al (2013) Drusen detection by confocal aperture-modulated infrared scanning laser ophthalmoscopy. Br J Ophthalmol 97:285–290. https://doi.org/10.1136/bjophthalmol-2012-302575
34. Delori FC, Dorey CK, Staurenghi G et al (1995) In vivo fluorescence of the ocular fundus exhibits retinal pigment epithelium lipofuscin characteristics. Invest Ophthalmol Vis Sci 36:718–729
35. Yung M, Klufas MA, Sarraf D (2016) Clinical applications of fundus autofluorescence in retinal disease. Int J Retina Vitr 2:12. https://doi.org/10.1186/s40942-016-0035-x
36. Warburton S, Davis WE, Southwick K et al (2007) Proteomic and phototoxic characterization of melanolipofuscin: correlation to disease and model for its origin. Mol Vis 13:318–329
37. Holz FG, Steinberg JS, Göbel A et al (2015) Fundus autofluorescence imaging in dry AMD: 2014 Jules Gonin lecture of the Retina Research Foundation. Graefes Arch Clin Exp Ophthalmol Albrecht Von Graefes Arch Klin Exp Ophthalmol 253:7–16. https://doi.org/10.1007/s00417-014-2858-1
38. Bindewald A, Bird AC, Dandekar SS et al (2005) Classification of fundus autofluorescence patterns in early age-related macular disease. Invest Ophthalmol Vis Sci 46:3309–3314. https://doi.org/10.1167/iovs.04-0430
39. Einbock W, Moessner A, Schnurrbusch UEK et al (2005) Changes in fundus autofluorescence in patients with age-related maculopathy. Correlation to visual function: a prospective study. Graefes Arch Clin Exp Ophthalmol Albrecht Von Graefes Arch Klin Exp Ophthalmol 243:300–305. https://doi.org/10.1007/s00417-004-1027-3
40. Batioğlu F, Demirel S, Ozmert E et al (2014) Autofluorescence patterns as a predictive factor for neovascularization. Optom Vis Sci Off Publ Am Acad Optom 91:950–955. https://doi.org/10.1097/OPX.0000000000000321
41. Landa G, Rosen RB, Pilavas J, Garcia PMT (2012) Drusen characteristics revealed by spectral-domain optical coherence tomography and their corresponding fundus autofluorescence appearance in dry age-related macular degeneration. Ophthalmic Res 47:81–86. https://doi.org/10.1159/000324988
42. Lois N, Owens SL, Coco R et al (2002) Fundus autofluorescence in patients with age-related macular degeneration and high risk of visual loss. Am J Ophthalmol 133:341–349
43. Delori FC, Fleckner MR, Goger DG et al (2000) Autofluorescence distribution associated with drusen in age-related macular degeneration. Invest Ophthalmol Vis Sci 41:496–504
44. Mrejen S, Sarraf D, Mukkamala SK, Freund KB (2013) Multimodal imaging of pigment epithelial detachment: a guide to evaluation. Retina Phila PA 33:1735–1762. https://doi.org/10.1097/IAE.0b013e3182993f66
45. Mimoun G, Soubrane G, Coscas G (1990) Macular drusen. J Fr Ophtalmol 13:511–530
46. Schmitz-Valckenberg S, Steinberg JS, Fleckenstein M et al (2010) Combined confocal scanning laser ophthalmoscopy and spectral-domain optical coherence tomography imaging of reticular drusen associated with age-related macular degeneration. Ophthalmology 117:1169–1176. https://doi.org/10.1016/j.ophtha.2009.10.044
47. Vaclavik V, Vujosevic S, Dandekar SS et al (2008) Autofluorescence imaging in age-related macular degeneration complicated by choroidal neovascularization: a prospective study. Ophthalmology 115:342–346. https://doi.org/10.1016/j.ophtha.2007.04.023

48. McBain VA, Townend J, Lois N (2007) Fundus autofluorescence in exudative age-related macular degeneration. Br J Ophthalmol 91:491–496. https://doi.org/10.1136/bjo.2006.095109
49. Hu Z, Medioni GG, Hernandez M, Sadda SR (2015) Automated segmentation of geographic atrophy in fundus autofluorescence images using supervised pixel classification. J Med Imaging Bellingham Wash 2:014501. https://doi.org/10.1117/1.JMI.2.1.014501
50. Zanzottera EC, Messinger JD, Ach T et al (2015) The project MACULA retinal pigment epithelium grading system for histology and optical coherence tomography in age-related macular degeneration. Invest Ophthalmol Vis Sci 56:3253–3268. https://doi.org/10.1167/iovs.15-16431
51. Gocho K, Sarda V, Falah S et al (2013) Adaptive optics imaging of geographic atrophy. Invest Ophthalmol Vis Sci 54:3673–3680. https://doi.org/10.1167/iovs.12-10672
52. Rudolf M, Vogt SD, Curcio CA et al (2013) Histologic basis of variations in retinal pigment epithelium autofluorescence in eyes with geographic atrophy. Ophthalmology 120:821–828. https://doi.org/10.1016/j.ophtha.2012.10.007
53. Pilotto E, Benetti E, Convento E et al (2013) Microperimetry, fundus autofluorescence, and retinal layer changes in progressing geographic atrophy. Can J Ophthalmol 48:386–393. https://doi.org/10.1016/j.jcjo.2013.03.022
54. Kuehlewein L, Dustin L, Sagong M et al (2016) Predictors of macular atrophy detected by fundus autofluorescence in patients with neovascular age-related macular degeneration after long-term Ranibizumab treatment. Ophthalmic Surg Lasers Imaging Retina 47:224–231. https://doi.org/10.3928/23258160-20160229-04
55. Lindner M, Böker A, Mauschitz MM et al (2015) Directional kinetics of geographic atrophy progression in age-related macular degeneration with foveal sparing. Ophthalmology 122:1356–1365. https://doi.org/10.1016/j.ophtha.2015.03.027
56. Holz FG, Bindewald-Wittich A, Fleckenstein M et al (2007) Progression of geographic atrophy and impact of fundus autofluorescence patterns in age-related macular degeneration. Am J Ophthalmol 143:463–472. https://doi.org/10.1016/j.ajo.2006.11.041
57. Schmitz-Valckenberg S, Brinkmann CK, Alten F et al (2011) Semiautomated image processing method for identification and quantification of geographic atrophy in age-related macular degeneration. Invest Ophthalmol Vis Sci 52:7640–7646. https://doi.org/10.1167/iovs.11-7457
58. Pilotto E, Guidolin F, Convento E et al (2013) Fundus autofluorescence and microperimetry in progressing geographic atrophy secondary to age-related macular degeneration. Br J Ophthalmol 97:622–626. https://doi.org/10.1136/bjophthalmol-2012-302633
59. Panorgias A, Zawadzki RJ, Capps AG et al (2013) Multimodal assessment of microscopic morphology and retinal function in patients with geographic atrophy. Invest Ophthalmol Vis Sci 54:4372–4384. https://doi.org/10.1167/iovs.12-11525
60. Sato T, Suzuki M, Ooto S, Spaide RF (2015) Multimodal imaging findings and multimodal vision testing in neovascular age-related macular degeneration. Retina Phila PA 35:1292–1302. https://doi.org/10.1097/IAE.0000000000000505
61. Kumar N, Mrejen S, Fung AT-C et al (2013) Retinal pigment epithelial cell loss assessed by fundus autofluorescence imaging in neovascular age-related macular degeneration. Ophthalmology 120:334–341. https://doi.org/10.1016/j.ophtha.2012.07.076
62. Keilhauer CN, Delori FC (2006) Near-infrared autofluorescence imaging of the fundus: visualization of ocular melanin. Invest Ophthalmol Vis Sci 47:3556–3564. https://doi.org/10.1167/iovs.06-0122
63. Weinberger AWA, Lappas A, Kirschkamp T et al (2006) Fundus near infrared fluorescence correlates with fundus near infrared reflectance. Invest Ophthalmol Vis Sci 47:3098–3108. https://doi.org/10.1167/iovs.05-1104
64. Skondra D, Papakostas TD, Hunter R, Vavvas DG (2012) Near infrared autofluorescence imaging of retinal diseases. Semin Ophthalmol 27:202–208. https://doi.org/10.3109/08820538.2012.708806
65. Heiferman MJ, Fawzi AA (2016) Discordance between blue-light autofluorescence and near-infrared autofluorescence in age-related macular degeneration. Retina Phila PA 36:S137–S146. https://doi.org/10.1097/IAE.0000000000001254
66. Pilotto E, Vujosevic S, Melis R et al (2011) Short wavelength fundus autofluorescence versus near-infrared fundus autofluorescence, with microperimetric correspondence, in patients with geographic atrophy due to age-related macular degeneration. Br J Ophthalmol 95:1140–1144. https://doi.org/10.1136/bjo.2010.187344
67. Wolf-Schnurrbusch UEK, Wittwer VV, Ghanem R et al (2011) Blue-light versus green-light autofluorescence: lesion size of areas of geographic atrophy. Invest Ophthalmol Vis Sci 52:9497–9502. https://doi.org/10.1167/iovs.11-8346
68. Yehoshua Z, de Amorim Garcia Filho CA, Nunes RP et al (2015) Comparison of geographic atrophy growth rates using different imaging modalities in the COMPLETE Study. Ophthalmic Surg Lasers Imaging Retina 46:413–422. https://doi.org/10.3928/23258160-20150422-03
69. Pfau M, Goerdt L, Schmitz-Valckenberg S et al (2017) Green-Light autofluorescence versus combined blue-light autofluorescence and near-infrared reflectance imaging in geographic atrophy secondary to age-related macular degeneration. Invest

Ophthalmol Vis Sci 58:BIO121–BIO130. https://doi.org/10.1167/iovs.17-21764
70. Schweitzer D, Schenke S, Hammer M et al (2007) Towards metabolic mapping of the human retina. Microsc Res Tech 70:410–419. https://doi.org/10.1002/jemt.20427
71. Borrelli E, Lei J, Balasubramanian S et al (2018) Green emission fluorophores in eyes with atrophic age-related macular degeneration: a colour fundus autofluorescence pilot study. Br J Ophthalmol 102:827–832. https://doi.org/10.1136/bjophthalmol-2017-310881
72. Borrelli E, Nittala MG, Abdelfattah NS et al (2018) Comparison of short-wavelength blue-light autofluorescence and conventional blue-light autofluorescence in geographic atrophy. Br J Ophthalmol. https://doi.org/10.1136/bjophthalmol-2018-311849
73. Delori F, Greenberg JP, Woods RL et al (2011) Quantitative measurements of autofluorescence with the scanning laser ophthalmoscope. Invest Ophthalmol Vis Sci 52:9379–9390. https://doi.org/10.1167/iovs.11-8319
74. Greenberg JP, Duncker T, Woods RL et al (2013) Quantitative fundus autofluorescence in healthy eyes. Invest Ophthalmol Vis Sci 54:5684–5693. https://doi.org/10.1167/iovs.13-12445
75. Eandi CM, Nassisi M, Lavia C et al (2017) Macular pigment density and quantitative fundus autofluorescence in young healthy subjects. Invest Ophthalmol Vis Sci 58:2284–2290. https://doi.org/10.1167/iovs.16-20510
76. Armenti ST, Greenberg JP, Smith RT (2016) Quantitative fundus autofluorescence for the evaluation of retinal diseases. J Vis Exp JoVE. https://doi.org/10.3791/53577
77. Burke TR, Duncker T, Woods RL et al (2014) Quantitative fundus autofluorescence in recessive Stargardt disease. Invest Ophthalmol Vis Sci 55:2841–2852. https://doi.org/10.1167/iovs.13-13624
78. Sparrow JR, Duncker T, Woods R, Delori FC (2016) Quantitative fundus autofluorescence in best vitelliform macular dystrophy: RPE Lipofuscin is not increased in non-lesion areas of retina. Adv Exp Med Biol 854:285–290. https://doi.org/10.1007/978-3-319-17121-0_38
79. Gliem M, Müller PL, Finger RP et al (2016) Quantitative fundus autofluorescence in early and intermediate age-related macular degeneration. JAMA Ophthalmol 134:817–824. https://doi.org/10.1001/jamaophthalmol.2016.1475
80. Dysli C, Quellec G, Abegg M et al (2014) Quantitative analysis of fluorescence lifetime measurements of the macula using the fluorescence lifetime imaging ophthalmoscope in healthy subjects. Invest Ophthalmol Vis Sci 55:2106–2113. https://doi.org/10.1167/iovs.13-13627
81. Dysli C, Wolf S, Hatz K, Zinkernagel MS (2016) Fluorescence lifetime imaging in Stargardt disease: potential marker for disease progression. Invest Ophthalmol Vis Sci 57:832–841. https://doi.org/10.1167/iovs.15-18033
82. Dysli C, Wolf S, Zinkernagel MS (2016) Autofluorescence lifetimes in geographic atrophy in patients with age-related macular degeneration. Invest Ophthalmol Vis Sci 57:2479–2487. https://doi.org/10.1167/iovs.15-18381
83. Dysli C, Fink R, Wolf S, Zinkernagel MS (2017) Fluorescence lifetimes of Drusen in age-related macular degeneration. Invest Ophthalmol Vis Sci 58:4856–4862. https://doi.org/10.1167/iovs.17-22184
84. (1991) Subfoveal neovascular lesions in age-related macular degeneration. Guidelines for evaluation and treatment in the macular photocoagulation study. Macular Photocoagulation Study Group. Arch Ophthalmol Chic Ill 1960 109:1242–1257
85. Novotny HR, Alvis DL (1961) A method of photographing fluorescence in circulating blood in the human retina. Circulation 24:82–86
86. Prenner JL, Rosenblatt BJ, Tolentino MJ et al (2003) Risk factors for choroidal neovascularization and vision loss in the fellow eye study of CNVPT. Retina Phila PA 23:307–314
87. Age-Related Macular Degeneration PPP - Updated 2015 - American Academy of Ophthalmology. https://www.aao.org/preferred-practice-pattern/age-related-macular-degeneration-ppp-2015. Accessed 21 Jul 2018
88. Freund KB, Zweifel SA, Engelbert M (2010) Do we need a new classification for choroidal neovascularization in age-related macular degeneration? Retina Phila PA 30:1333–1349. https://doi.org/10.1097/IAE.0b013e3181e7976b
89. Jung JJ, Chen CY, Mrejen S et al (2014) The incidence of neovascular subtypes in newly diagnosed neovascular age-related macular degeneration. Am J Ophthalmol 158:769–779.e2. https://doi.org/10.1016/j.ajo.2014.07.006
90. Gass JD (1984) Serous retinal pigment epithelial detachment with a notch. A sign of occult choroidal neovascularization. Retina Phila PA 4:205–220
91. Hartnett ME, Weiter JJ, Garsd A, Jalkh AE (1992) Classification of retinal pigment epithelial detachments associated with drusen. Graefes Arch Clin Exp Ophthalmol Albrecht Von Graefes Arch Klin Exp Ophthalmol 230:11–19
92. Dansingani KK, Gal-Or O, Sadda SR et al (2018) Understanding aneurysmal type 1 neovascularization (polypoidal choroidal vasculopathy): a lesson in the taxonomy of 'expanded spectra' – a review. Clin Experiment Ophthalmol 46:189–200. https://doi.org/10.1111/ceo.13114
93. Kim JH, Chang YS, Kim JW et al (2016) Diagnosis of type 3 neovascularization based on optical coherence tomography images. Retina Phila PA

36:1506–1515. https://doi.org/10.1097/IAE.0000000000000932
94. Yannuzzi LA, Freund KB, Takahashi BS (2008) Review of retinal angiomatous proliferation or type 3 neovascularization. Retina Phila PA 28:375–384. https://doi.org/10.1097/IAE.0b013e3181619c55
95. Xu L, Mrejen S, Jung JJ et al (2015) Geographic atrophy in patients receiving anti-vascular endothelial growth factor for neovascular age-related macular degeneration. Retina Phila PA 35:176–186. https://doi.org/10.1097/IAE.0000000000000374
96. Comparison of Age-related Macular Degeneration Treatments Trials (CATT) Research Group, Martin DF, Maguire MG et al (2012) Ranibizumab and bevacizumab for treatment of neovascular age-related macular degeneration: two-year results. Ophthalmology 119:1388–1398. https://doi.org/10.1016/j.ophtha.2012.03.053
97. Chakravarthy U, Harding SP, Rogers CA et al (2013) Alternative treatments to inhibit VEGF in age-related choroidal neovascularisation: 2-year findings of the IVAN randomised controlled trial. Lancet Lond Engl 382:1258–1267. https://doi.org/10.1016/S0140-6736(13)61501-9
98. Grunwald JE, Daniel E, Huang J et al (2014) Risk of geographic atrophy in the comparison of age-related macular degeneration treatments trials. Ophthalmology 121:150–161. https://doi.org/10.1016/j.ophtha.2013.08.015
99. Khurana RN, Dupas B, Bressler NM (2010) Agreement of time-domain and spectral-domain optical coherence tomography with fluorescein leakage from choroidal neovascularization. Ophthalmology 117:1376–1380. https://doi.org/10.1016/j.ophtha.2009.11.039
100. Holz FG, Bellmann C, Rohrschneider K et al (1998) Simultaneous confocal scanning laser fluorescein and indocyanine green angiography. Am J Ophthalmol 125:227–236
101. Spaide RF, Yannuzzi LA, Slakter JS et al (1995) Indocyanine green videoangiography of idiopathic polypoidal choroidal vasculopathy. Retina Phila PA 15:100–110
102. Spaide RF, Koizumi H, Pozzoni MC, Pozonni MC (2008) Enhanced depth imaging spectral-domain optical coherence tomography. Am J Ophthalmol 146:496–500. https://doi.org/10.1016/j.ajo.2008.05.032
103. Wong CW, Yanagi Y, Lee W-K, et al (2016) Age-related macular degeneration and polypoidal choroidal vasculopathy in Asians. Prog Retin Eye Res 53:107–139. https://doi.org/10.1016/j.preteyeres.2016.04.002
104. Spaide RF (2018) Disease expression in nonexudative age-related macular degeneration varies with choroidal thickness. Retina Phila PA 38:708–716. https://doi.org/10.1097/IAE.0000000000001689
105. Giani A, Pellegrini M, Carini E et al (2012) The dark atrophy with indocyanine green angiography in Stargardt disease. Invest Ophthalmol Vis Sci 53:3999–4004. https://doi.org/10.1167/iovs.11-9258
106. Pauleikhoff D, Spital G, Radermacher M et al (1999) A fluorescein and indocyanine green angiographic study of choriocapillaris in age-related macular disease. Arch Ophthalmol Chic Ill 1960 117:1353–1358
107. Mori K, Gehlbach PL, Ito YN, Yoneya S (2005) Decreased arterial dye-filling and venous dilation in the macular choroid associated with age-related macular degeneration. Retina Phila PA 25:430–437
108. Bonnay G, Nguyen F, Meunier I et al (2011) Screening for retinal detachment using wide-field retinal imaging. J Fr Ophtalmol 34:482–485. https://doi.org/10.1016/j.jfo.2011.02.012
109. Staurenghi G, Viola F, Mainster MA et al (2005) Scanning laser ophthalmoscopy and angiography with a wide-field contact lens system. Arch Ophthalmol Chic Ill 1960 123:244–252. https://doi.org/10.1001/archopht.123.2.244
110. Espina M, Barteselli G, Ma F et al (2014) Noncontact Ultra-wide field Lens system by Heidelberg Spectralis. Invest Ophthalmol Vis Sci 55:1615–1615
111. Csutak A, Lengyel I, Jonasson F et al (2010) Agreement between image grading of conventional (45°) and ultra wide-angle (200°) digital images in the macula in the Reykjavik eye study. Eye Lond Engl 24:1568–1575. https://doi.org/10.1038/eye.2010.85
112. Lengyel I, Csutak A, Florea D et al (2015) A population-based ultra-widefield digital image grading study for age-related macular degeneration-like lesions at the peripheral retina. Ophthalmology 122:1340–1347. https://doi.org/10.1016/j.ophtha.2015.03.005
113. Bae K, Cho K, Kang SW et al (2017) Peripheral reticular pigmentary degeneration and choroidal vascular insufficiency, studied by ultra wide-field fluorescein angiography. PLoS One 12:e0170526. https://doi.org/10.1371/journal.pone.0170526
114. Shuler RK, Schmidt S, Gallins P et al (2008) Peripheral reticular pigmentary change is associated with complement factor H polymorphism (Y402H) in age-related macular degeneration. Ophthalmology 115:520–524. https://doi.org/10.1016/j.ophtha.2007.06.021
115. Tan CS, Heussen F, Sadda SR (2013) Peripheral autofluorescence and clinical findings in neovascular and non-neovascular age-related macular degeneration. Ophthalmology 120:1271–1277. https://doi.org/10.1016/j.ophtha.2012.12.002
116. Duisdieker V, Fleckenstein M, Zilkens KM et al (2015) Long-term follow-up of fundus autofluorescence imaging using wide-field scanning laser ophthalmoscopy. Ophthalmol J Int Ophtalmol Int J Ophthalmol Z Augenheilkd 234:218–226. https://doi.org/10.1159/000439358
117. Huang D, Swanson EA, Lin CP et al (1991) Optical coherence tomography. Science 254:1178–1181
118. Drexler W, Morgner U, Ghanta RK et al (2001) Ultrahigh-resolution ophthalmic optical coherence

tomography. Nat Med 7:502–507. https://doi.org/10.1038/86589
119. Fujimoto J, Swanson E (2016) The development, commercialization, and impact of optical coherence tomography. Invest Ophthalmol Vis Sci 57:OCT1–OCT13. https://doi.org/10.1167/iovs.16-19963
120. Lane M, Moult EM, Novais EA et al (2016) Visualizing the choriocapillaris under drusen: comparing 1050-nm swept-source versus 840-nm spectral-domain optical coherence tomography angiography. Invest Ophthalmol Vis Sci 57:585–590. https://doi.org/10.1167/iovs.15-18915
121. Choma M, Sarunic M, Yang C, Izatt J (2003) Sensitivity advantage of swept source and Fourier domain optical coherence tomography. Opt Express 11:2183–2189
122. Fleckenstein M, Mitchell P, Freund KB et al (2018) The progression of geographic atrophy secondary to age-related macular degeneration. Ophthalmology 125:369–390. https://doi.org/10.1016/j.ophtha.2017.08.038
123. Ouyang Y, Heussen FM, Hariri A et al (2013) Optical coherence tomography-based observation of the natural history of drusenoid lesion in eyes with dry age-related macular degeneration. Ophthalmology 120:2656–2665. https://doi.org/10.1016/j.ophtha.2013.05.029
124. Schlanitz FG, Baumann B, Kundi M et al (2017) Drusen volume development over time and its relevance to the course of age-related macular degeneration. Br J Ophthalmol 101:198–203. https://doi.org/10.1136/bjophthalmol-2016-308422
125. Yehoshua Z, Wang F, Rosenfeld PJ et al (2011) Natural history of drusen morphology in age-related macular degeneration using spectral domain optical coherence tomography. Ophthalmology 118:2434–2441. https://doi.org/10.1016/j.ophtha.2011.05.008
126. Querques G, Souied EH (2015) Vascularized drusen: slowly progressive type 1 neovascularization mimicking drusenoid retinal pigment epithelium elevation. Retina Phila PA 35:2433–2439. https://doi.org/10.1097/IAE.0000000000000761
127. Suzuki M, Curcio CA, Mullins RF, Spaide RF (2015) Refractile drusen: clinical imaging and candidate histology. Retina Phila PA 35:859–865. https://doi.org/10.1097/IAE.0000000000000503
128. Spaide RF (2018) Improving the age-related macular degeneration construct: a new classification system. Retina Phila PA 38:891–899. https://doi.org/10.1097/IAE.0000000000001732
129. Nassisi M, Lei J, Abdelfattah NS et al (2019) OCT risk factors for development of late age-related macular degeneration in the fellow eyes of patients enrolled in the HARBOR study. Ophthalmology. https://doi.org/10.1016/j.ophtha.2019.05.016
130. Sadda SR, Guymer R, Holz FG et al (2017) Consensus definition for atrophy associated with age-related macular degeneration on OCT: classification of atrophy report 3. Ophthalmology. https://doi.org/10.1016/j.ophtha.2017.09.028
131. Folgar FA, Yuan EL, Sevilla MB et al (2016) Drusen volume and retinal pigment epithelium abnormal thinning volume predict 2-year progression of age-related macular degeneration. Ophthalmology 123:39–50.e1. https://doi.org/10.1016/j.ophtha.2015.09.016
132. Nassisi M, Fan W, Shi Y et al (2018) Quantity of intraretinal hyperreflective foci in patients with intermediate age-related macular degeneration correlates with 1-year progression. Invest Ophthalmol Vis Sci 59:3431–3439. https://doi.org/10.1167/iovs.18-24143
133. Coscas F, Querques G, Forte R et al (2012) Combined fluorescein angiography and spectral-domain optical coherence tomography imaging of classic choroidal neovascularization secondary to age-related macular degeneration before and after intravitreal ranibizumab injections. Retina Phila PA 32:1069–1076. https://doi.org/10.1097/IAE.0b013e318240a529
134. Nagiel A, Sarraf D, Sadda SR et al (2015) Type 3 neovascularization: evolution, association with pigment epithelial detachment, and treatment response as revealed by spectral domain optical coherence tomography. Retina Phila PA 35:638–647. https://doi.org/10.1097/IAE.0000000000000488
135. De Salvo G, Vaz-Pereira S, Keane PA et al (2014) Sensitivity and specificity of spectral-domain optical coherence tomography in detecting idiopathic polypoidal choroidal vasculopathy. Am J Ophthalmol 158:1228–1238.e1. https://doi.org/10.1016/j.ajo.2014.08.025
136. Busbee BG, Ho AC, Brown DM et al (2013) Twelve-month efficacy and safety of 0.5 mg or 2.0 mg ranibizumab in patients with subfoveal neovascular age-related macular degeneration. Ophthalmology 120:1046–1056. https://doi.org/10.1016/j.ophtha.2012.10.014
137. Schmidt-Erfurth U, Waldstein SM (2016) A paradigm shift in imaging biomarkers in neovascular age-related macular degeneration. Prog Retin Eye Res 50:1–24. https://doi.org/10.1016/j.preteyeres.2015.07.007
138. Yehoshua Z, Rosenfeld PJ, Gregori G et al (2011) Progression of geographic atrophy in age-related macular degeneration imaged with spectral domain optical coherence tomography. Ophthalmology 118:679–686. https://doi.org/10.1016/j.ophtha.2010.08.018
139. Wu Z, Luu CD, Ayton LN et al (2015) Fundus autofluorescence characteristics of nascent geographic atrophy in age-related macular degeneration. Invest Ophthalmol Vis Sci 56:1546–1552. https://doi.org/10.1167/iovs.14-16211
140. Moussa K, Lee JY, Stinnett SS, Jaffe GJ (2013) Spectral domain optical coherence tomography-determined morphologic predictors of age-related macular degeneration-associated geographic atrophy

progression. Retina Phila PA 33:1590–1599. https://doi.org/10.1097/IAE.0b013e31828d6052
141. Ebneter A, Jaggi D, Abegg M et al (2016) Relationship between presumptive inner nuclear layer thickness and geographic atrophy progression in age-related macular degeneration. Invest Ophthalmol Vis Sci 57:OCT299–OCT306. https://doi.org/10.1167/iovs.15-18865
142. Bearelly S, Chau FY, Koreishi A et al (2009) Spectral domain optical coherence tomography imaging of geographic atrophy margins. Ophthalmology 116:1762–1769. https://doi.org/10.1016/j.ophtha.2009.04.015
143. Lee JY, Folgar FA, Maguire MG et al (2014) Outer retinal tubulation in the comparison of age-related macular degeneration treatments trials (CATT). Ophthalmology 121:2423–2431. https://doi.org/10.1016/j.ophtha.2014.06.013
144. Litts KM, Messinger JD, Dellatorre K et al (2015) Clinicopathological correlation of outer retinal tubulation in age-related macular degeneration. JAMA Ophthalmol 133:609–612. https://doi.org/10.1001/jamaophthalmol.2015.126
145. Preti RC, Govetto A, Filho RGA et al (2018) Optical coherence tomography analysis of outer retinal tubulations: sequential evolution and pathophysiological insights. Retina Phila PA 38:1518–1525. https://doi.org/10.1097/IAE.0000000000001810
146. Hariri A, Nittala MG, Sadda SR (2015) Outer retinal tubulation as a predictor of the enlargement amount of geographic atrophy in age-related macular degeneration. Ophthalmology 122:407–413. https://doi.org/10.1016/j.ophtha.2014.08.035
147. Friedman E (1997) A hemodynamic model of the pathogenesis of age-related macular degeneration. Am J Ophthalmol 124:677–682
148. Grunwald JE, Hariprasad SM, DuPont J et al (1998) Foveolar choroidal blood flow in age-related macular degeneration. Invest Ophthalmol Vis Sci 39:385–390
149. Grunwald JE, Metelitsina TI, Dupont JC et al (2005) Reduced foveolar choroidal blood flow in eyes with increasing AMD severity. Invest Ophthalmol Vis Sci 46:1033–1038. https://doi.org/10.1167/iovs.04-1050
150. Sigler EJ, Randolph JC (2013) Comparison of macular choroidal thickness among patients older than age 65 with early atrophic age-related macular degeneration and normals. Invest Ophthalmol Vis Sci 54:6307–6313. https://doi.org/10.1167/iovs.13-12653
151. Govetto A, Sarraf D, Figueroa MS et al (2017) Choroidal thickness in non-neovascular versus neovascular age-related macular degeneration: a fellow eye comparative study. Br J Ophthalmol 101:764–769. https://doi.org/10.1136/bjophthalmol-2016-309281
152. Kim S-W, Oh J, Kwon S-S et al (2011) Comparison of choroidal thickness among patients with healthy eyes, early age-related maculopathy, neovascular age-related macular degeneration, central serous chorioretinopathy, and polypoidal choroidal vasculopathy. Retina Phila PA 31:1904–1911. https://doi.org/10.1097/IAE.0b013e31821801c5
153. Chung SE, Kang SW, Lee JH, Kim YT (2011) Choroidal thickness in polypoidal choroidal vasculopathy and exudative age-related macular degeneration. Ophthalmology 118:840–845. https://doi.org/10.1016/j.ophtha.2010.09.012
154. White B, Pierce M, Nassif N et al (2003) In vivo dynamic human retinal blood flow imaging using ultra-high-speed spectral domain optical coherence tomography. Opt Express 11:3490–3497
155. Zhang J, Chen Z (2005) In vivo blood flow imaging by a swept laser source based Fourier domain optical Doppler tomography. Opt Express 13:7449–7457. https://doi.org/10.1364/OPEX.13.007449
156. Spaide RF, Fujimoto JG, Waheed NK et al (2018) Optical coherence tomography angiography. Prog Retin Eye Res 64:1–55. https://doi.org/10.1016/j.preteyeres.2017.11.003
157. Curcio CA, Messinger JD, Sloan KR et al (2013) Subretinal drusenoid deposits in non-neovascular age-related macular degeneration: morphology, prevalence, topography, and biogenesis model. Retina Phila PA 33:265–276. https://doi.org/10.1097/IAE.0b013e31827e25e0
158. Mullins RF, Johnson MN, Faidley EA et al (2011) Choriocapillaris vascular dropout related to density of drusen in human eyes with early age-related macular degeneration. Invest Ophthalmol Vis Sci 52:1606–1612. https://doi.org/10.1167/iovs.10-6476
159. Borrelli E, Uji A, Sarraf D, Sadda SR (2017) Alterations in the choriocapillaris in intermediate age-related macular degeneration. Invest Ophthalmol Vis Sci 58:4792–4798. https://doi.org/10.1167/iovs.17-22360
160. Querques G, Querques L, Forte R et al (2012) Choroidal changes associated with reticular pseudodrusen. Invest Ophthalmol Vis Sci 53:1258–1263. https://doi.org/10.1167/iovs.11-8907
161. Grewal DS, Chou J, Rollins SD, Fawzi AA (2014) A pilot quantitative study of topographic correlation between reticular pseudodrusen and the choroidal vasculature using en face optical coherence tomography. PLoS One 9:e92841. https://doi.org/10.1371/journal.pone.0092841
162. Borrelli E, Mastropasqua R, Senatore A et al (2018) Impact of choriocapillaris flow on multifocal electroretinography in intermediate age-related macular degeneration eyes. Invest Ophthalmol Vis Sci 59:25–30. https://doi.org/10.1167/iovs.18-23943
163. Toto L, Borrelli E, Di Antonio L et al (2016) Retinal vascular plexuses' changes in dry age-related macular degeneration, evaluated by means of optical coherence tomography angiography. Retina Phila PA 36:1566–1572. https://doi.org/10.1097/IAE.0000000000000962
164. Sacconi R, Corbelli E, Carnevali A et al (2017) Optical coherence tomography angiography in

geographic atrophy. Retina Phila PA. https://doi.org/10.1097/IAE.0000000000001873
165. Nassisi M, Shi Y, Fan W et al (2018) Choriocapillaris impairment around the atrophic lesions in patients with geographic atrophy: a swept-source optical coherence tomography angiography study. Br J Ophthalmol. https://doi.org/10.1136/bjophthalmol-2018-312643
166. Moult EM, Waheed NK, Novais EA et al (2016) Swept-source optical coherence tomography angiography reveals choriocapillaris alterations in eyes with nascent geographic atrophy and drusen-associated geographic atrophy. Retina Phila PA 1:S2–S11. https://doi.org/10.1097/IAE.0000000000001287
167. Schlingemann RO (2004) Role of growth factors and the wound healing response in age-related macular degeneration. Graefes Arch Clin Exp Ophthalmol Albrecht Von Graefes Arch Klin Exp Ophthalmol 242:91–101. https://doi.org/10.1007/s00417-003-0828-0
168. Choi W, Moult EM, Waheed NK et al (2015) Ultrahigh-speed, swept-source optical coherence tomography angiography in nonexudative age-related macular degeneration with geographic atrophy. Ophthalmology 122:2532–2544. https://doi.org/10.1016/j.ophtha.2015.08.029
169. Biesemeier A, Taubitz T, Julien S et al (2014) Choriocapillaris breakdown precedes retinal degeneration in age-related macular degeneration. Neurobiol Aging 35:2562–2573. https://doi.org/10.1016/j.neurobiolaging.2014.05.003
170. Carnevali A, Cicinelli MV, Capuano V et al (2016) Optical coherence tomography angiography: a useful tool for diagnosis of treatment-naïve quiescent choroidal neovascularization. Am J Ophthalmol 169:189–198. https://doi.org/10.1016/j.ajo.2016.06.042
171. Coscas GJ, Lupidi M, Coscas F et al (2015) Optical coherence tomography angiography versus traditional multimodal imaging in assessing the activity of exudative age-related macular degeneration: a new diagnostic challenge. Retina Phila PA 35:2219–2228. https://doi.org/10.1097/IAE.0000000000000766
172. Inoue M, Jung JJ, Balaratnasingam C et al (2016) A comparison between optical coherence tomography angiography and fluorescein angiography for the imaging of type 1 neovascularization. Invest Ophthalmol Vis Sci 57:OCT314–OCT323. https://doi.org/10.1167/iovs.15-18900
173. Souied EH, El Ameen A, Semoun O et al (2016) Optical coherence tomography angiography of type 2 neovascularization in age-related macular degeneration. Dev Ophthalmol 56:52–56. https://doi.org/10.1159/000442777
174. Gong J, Yu S, Gong Y et al (2016) The diagnostic accuracy of optical coherence tomography angiography for neovascular age-related macular degeneration: a comparison with fundus fluorescein angiography. J Ophthalmol 2016:7521478. https://doi.org/10.1155/2016/7521478
175. Kuehlewein L, Bansal M, Lenis TL et al (2015) Optical coherence tomography angiography of type 1 neovascularization in age-related macular degeneration. Am J Ophthalmol 160:739–748.e2. https://doi.org/10.1016/j.ajo.2015.06.030
176. Spaide RF, Fujimoto JG, Waheed NK (2015) Image artifacts in optical coherence tomography angiography. Retina 35:2163–2180. https://doi.org/10.1097/IAE.0000000000000765
177. Bhutto I, Lutty G (2012) Understanding age-related macular degeneration (AMD): relationships between the photoreceptor/retinal pigment epithelium/Bruch's membrane/choriocapillaris complex. Mol Aspects Med 33:295–317. https://doi.org/10.1016/j.mam.2012.04.005
178. Liang MC, de Carlo TE, Baumal CR et al (2016) Correlation of spectral domain optical coherence tomography angiography and clinical activity in neovascular age-related macular degeneration. Retina 36:2265. https://doi.org/10.1097/IAE.0000000000001102
179. Falavarjani KG, Iafe NA, Hubschman J-P et al (2017) Optical coherence tomography angiography analysis of the foveal avascular zone and macular vessel density after anti-VEGF therapy in eyes with diabetic macular edema and retinal vein occlusion. Invest Ophthalmol Vis Sci 58:30–34. https://doi.org/10.1167/iovs.16-20579
180. Zhang A, Zhang Q, Wang RK (2015) Minimizing projection artifacts for accurate presentation of choroidal neovascularization in OCT microangiography. Biomed Opt Express 6:4130–4143. https://doi.org/10.1364/BOE.6.004130
181. Cole ED, Moult EM, Dang S et al (2017) The definition, rationale, and effects of thresholding in OCT angiography. Ophthalmol Retina 1:435–447. https://doi.org/10.1016/j.oret.2017.01.019
182. de Carlo TE, Bonini Filho MA, Chin AT et al (2015) Spectral-domain optical coherence tomography angiography of choroidal neovascularization. Ophthalmology 122:1228–1238. https://doi.org/10.1016/j.ophtha.2015.01.029
183. Filho MAB, de Carlo TE, Ferrara D et al (2015) Association of choroidal neovascularization and central serous chorioretinopathy with optical coherence tomography angiography. JAMA Ophthalmol 133:899–906. https://doi.org/10.1001/jamaophthalmol.2015.1320
184. Bloom SM, Singal IP (2011) The outer Bruch membrane layer: a previously undescribed spectral-domain optical coherence tomography finding. Retina 31:316–323. https://doi.org/10.1097/IAE.0b013e3181ed8c9a
185. Choi W, Mohler KJ, Potsaid B et al (2013) Choriocapillaris and choroidal microvasculature imaging with ultrahigh speed OCT angiography. PLoS One 8:

e81499. https://doi.org/10.1371/journal.pone.0081499
186. McLeod DS, Grebe R, Bhutto I et al (2009) Relationship between RPE and choriocapillaris in age-related macular degeneration. Invest Ophthalmol Vis Sci 50:4982–4991. https://doi.org/10.1167/iovs.09-3639
187. Pepple K, Mruthyunjaya P (2011) Retinal pigment epithelial detachments in age-related macular degeneration: classification and therapeutic options. Semin Ophthalmol 26:198–208. https://doi.org/10.3109/08820538.2011.570850
188. Liang J, Williams DR, Miller DT (1997) Supernormal vision and high-resolution retinal imaging through adaptive optics. J Opt Soc Am A Opt Image Sci Vis 14:2884–2892
189. Roorda A, Romero-Borja F, Donnelly Iii W et al (2002) Adaptive optics scanning laser ophthalmoscopy. Opt Express 10:405–412
190. Talcott KE, Ratnam K, Sundquist SM et al (2011) Longitudinal study of cone photoreceptors during retinal degeneration and in response to ciliary neurotrophic factor treatment. Invest Ophthalmol Vis Sci 52:2219–2226. https://doi.org/10.1167/iovs.10-6479
191. Zhang Y, Poonja S, Roorda A (2006) MEMS-based adaptive optics scanning laser ophthalmoscopy. Opt Lett 31:1268–1270
192. Rossi EA, Rangel-Fonseca P, Parkins K et al (2013) In vivo imaging of retinal pigment epithelium cells in age related macular degeneration. Biomed Opt Express 4:2527–2539. https://doi.org/10.1364/BOE.4.002527
193. Boretsky A, Khan F, Burnett G et al (2012) In vivo imaging of photoreceptor disruption associated with age-related macular degeneration: a pilot study. Lasers Surg Med 44:603–610. https://doi.org/10.1002/lsm.22070
194. Zayit-Soudry S, Duncan JL, Syed R et al (2013) Cone structure imaged with adaptive optics scanning laser ophthalmoscopy in eyes with nonneovascular age-related macular degeneration. Invest Ophthalmol Vis Sci 54:7498–7509. https://doi.org/10.1167/iovs.13-12433
195. Brar M, Kozak I, Cheng L et al (2009) Correlation between spectral-domain optical coherence tomography and fundus autofluorescence at the margins of geographic atrophy. Am J Ophthalmol 148:439–444. https://doi.org/10.1016/j.ajo.2009.04.022
196. Roorda A, Williams DR (2002) Optical fiber properties of individual human cones. J Vis 2:404–412. https://doi.org/10.1167/2.5.4
197. Johnson PT, Brown MN, Pulliam BC et al (2005) Synaptic pathology, altered gene expression, and degeneration in photoreceptors impacted by drusen. Invest Ophthalmol Vis Sci 46:4788–4795. https://doi.org/10.1167/iovs.05-0767
198. Schuman SG, Koreishi AF, Farsiu S et al (2009) Photoreceptor layer thinning over drusen in eyes with age-related macular degeneration imaged in vivo with spectral-domain optical coherence tomography. Ophthalmology 116:488–496.e2. https://doi.org/10.1016/j.ophtha.2008.10.006
199. Querques G, Kamami-Levy C, Georges A et al (2016) Adaptive optics imaging of foveal sparing in geographic atrophy secondary to age-related macular degeneration. Retina Phila PA 36:247–254. https://doi.org/10.1097/IAE.0000000000000692